Electrode Material Dependence, Ion-Pairing and the Progressive Increase in Complexity of the α-$[S_2W_{18}O_{62}]^{4-/5-/6-/7-/8-/9-/10-}$ Reduction Processes in Acetonitrile Containing [n-Bu_4N][PF_6] as the Supporting Electrolyte

Md Anisur Rahman[a], Luke Gundry[a], Tadaharu Ueda[b, c], Alan M. Bond[a, d] * and Jie Zhang[a, d] *

[a] School of Chemistry, Monash University, Clayton, Victoria 3800, Australia

[b] Department of Marine Resource Science, Faculty of Agriculture and Marine Science, Kochi University, Kochi 780-8520, Japan

[c] Centre for Advanced Marine Core Research, Kochi University, Nankoku, 783-8502, Japan

[d] ARC Centre of Excellence for Electrochemical Science, Monash University, Clayton, Victoria 3800, Australia

ABSTRACT

Large amplitude Fourier transform alternating current (FTAC) voltammetry has been used to parameterise the electrode kinetics associated with the reduction of α-$[S_2W_{18}O_{62}]^{4-}$ in acetonitrile ([n-Bu_4N][PF_6]) at glassy carbon (GC), gold (Au) and platinum (Pt) electrodes by experimenter based heuristic and computer-assisted automated approaches. Electron transfer kinetics described by the Butler-Volmer relationship are faster at GC than that at the metal electrodes. Progressively increasing departure from ideality in the experimental versus simulated data comparisons were found with reduction processes that occur at more negative potentials and with higher electrolyte concentrations. Ion-pairing between α-$[S_2W_{18}O_{62}]^{4-}$ or its reduced forms and the electrolyte cation may contribute to non-conformance between theory and experiment. Electrochemical quartz crystal microbalance experiments along with other experiments reveal that adsorption of more extensively reduced species may modify the electrode surface and contribute to the asymmetry found in the reduction and oxidation components of the FTAC voltammetric data. Enhanced double layer effect at negative potentials also could explain why the level of non-ideality increases with reduction processes that occur at more negative potentials. The findings in this study are expected to apply to the voltammetric reduction of other very negatively charged polyoxometalates.

Keywords: Fourier transformed alternating current voltammetry, polyoxometalate electrochemistry, electrode kinetics, non-idealitiy, ion-pairing, adsorption.

1. INTRODUCTION

Polyoxometalates (POMs) are negatively charged inorganic oxide clusters having framework structures. In their commonly synthesised form, they are constructed from high oxidation state tungsten (VI), molybdenum (VI), vanadium (V) or other transition metals. As a consequence, their chemical and electrochemical reductive redox chemistry, to generate for example W(VI/V), Mo(VI/V/IV), V(V/IV) containing POM clusters is usually exceptionally rich. Typically, under voltammetric conditions in aprotic solvents they undergo a series of chemically and often electrochemically reversible one-electron reduction processes that represent metal based electron transfer reactions [1-2]. However, the electrons may be delocalised over all or part of POM framework rather than being localised on one metal centre [3-4].

The structure of the so-called Wells-Dawson structure of the α isomer of $[S_2W_{18}O_{62}]^{4-}$, which is of interest in this study, is provided in Figure 1. There are many possible isomeric forms of $[S_2W_{18}O_{62}]^{4-}$ [5] but it is assumed the fully symmetrical α structre remains intact during electrochemical reduction.

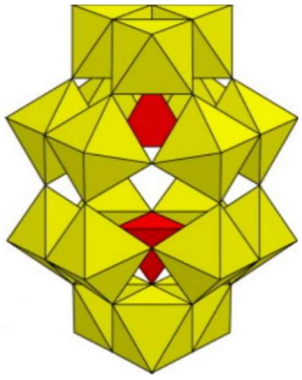

Figure 1. The structure of the α isomer of $[S_2W_{18}O_{62}]^{4-}$. Red and yellow represent the tetrahedral sulphate units and the octahedral tungstate units, respectively.

$[S_2W_{18}O_{62}]^{4-}$ contains 18 W(VI) metal centres, each of which in principle can be reduced to W(V) and then to W(IV) if a sufficiently strong chemical reductant is used or a sufficiently negative potential can be applied prior to the solvent limit under electrochemical conditions. Indeed, in the presence of proton reactions couped to electron transfer, which significantly facilitates reduction, 26 electrons have been added to the molybdenum analogue $[S_2Mo_{18}O_{62}]^{4-}$ [6]. In aprotic ionic liquids, that have a wide potential range in the negative potential region, as needed for extensive reduction of $[S_2W_{18}O_{62}]^{4-}$, six well-resolved one-electron reduction processes have been reported under voltammetric conditions at a glassy carbon (GC) electrode [7]. The electrochemistry of $[S_2W_{18}O_{62}]^{4-}$ in the dry acetonitrile (CH_3CN) with different supporting electrolytes [8-10], in the absence of deliberately added supporting electrolyte and in the presence of 5 (v/v) % water with and without acid also have been reported [7, 9] using a range of electrode materials with stationary, rotated and channel electrode configurations.

Table S1 summarises the formal reversible potentials (E_f^0) derived from analysis of DC cyclic voltammograms for the α-$[S_2W_{18}O_{62}]^{4-/5-/6-/7-/8-/9-/10-}$ processes (designated as I, II, III, IV, V and VI) using a range of electrodes, solvents and electrolyte. Clearly, the solvent plays a critical role [7]. Thus, with respect to molecular solvents, the most negative E_f^0 values (-0.437 V vs Fc/Fc^+ for process I) were obtained in dichloromethane (least polar solvent used) whereas use of water (most polar solvent used) gives a much more positive E_f^0 value (0.02 V vs Fc/Fc^+ for process I). Accordingly, since the polarity of CH_3CN lies between that of these two solvents, so do the E_f^0 values. In general, E_f^0 values are also very positive with use of ionic liquids. Moreover, E_f^0 values become more positive with higher electrolyte concentration because of increasing ion-pairing differences between the electrolyte cation ($[n\text{-}Bu_4N]^+$) and oxidised (e.g. α-$[S_2W_{18}O_{62}]^{4-}$) and reduced (e.g. α-$[S_2W_{18}O_{62}]^{5-}$) forms. Not surprisingly,

the purity of solvent, particularly with respect to water content also is critical [7] with more negative E_f^0 values obtained in carefully dried CH_3CN [7].

The above survey of literature reports implies that all processes associated with DC cyclic voltammetry of α-$[S_2W_{18}O_{62}]^{4-}$ at stationary macrodisc electrodes are ideal or close to ideal chemically or electrochemically reversible processes. Nevertheless, close inspection of data reveals significant departures from ideality under some conditions. Thus, while six well-resolved α-$[S_2W_{18}O_{62}]^{4-/5-/6-/7-/8-/9-/10-}$ processes have been reported at carbon based glassy carbon (GC) [8, 10] and boron doped diamond (BDD) [11] electrodes in acetonitrile under conditions of stationery electrode direct current (DC) cyclic voltammetry, it has been noted that only the first two are present at a rotating disc GC electrode [9]. Furthermore, in a quantitative electrode kinetic evaluation of the first two α-$[S_2W_{18}O_{62}]^{4-/5-/6-}$ processes by large amplitude Fourier transform alternating current (FTAC) voltammetry at GC, Au, Pt [8] and BDD [11] disc electrodes anomalous behaviour with respect to conformance to the Butler-Volmer model of electron transfer was detected, particularly with respect to the α-$[S_2W_{18}O_{62}]^{5-/6-}$ process at a Pt electrode. Anomalies with respect to theoretical predictions for simple one-electron reduction processes also have been noted in other studies with this electrode material when POM reduction processes occur at fairly negative potentials [1, 12]. Processes at Pt appear to have significantly slow electrode kinetics relative to the carbon and gold electrode cases. Under these circumstances, neglect of strong ion-paring that inevitably is a feature of POM chemistry [13-15], but rarely incorporated into parameterisation of the electrode kinetics, was hypothesized to be a possible contributing factor to discrepancies between Pt electrode experimental and simulated data [14].

In addition to ion-pairing, another special issue that also may arise with the extensive series of α-$[S_2W_{18}O_{62}]^{4-/5-/6-/7-/8-/9-/10}$ processes is that they encompass a very wide

potential range. This includes the very negative one near the solvent limit where the impact of the ion distribution in the electrode-solution double layer interfacial region [16-17] could be substantial. For example, with 0.10 M [*n*-Bu_4N] [PF_6] as the supporting electrolyte, the double layer region at and adjacent to a highly negatively charged electrode is expected to contain a very high concentration of the [*n*-Bu_4N]$^+$ cation. Accordingly, the double layer impact close to the negative solvent limit may be far more important than would apply at potentials near to the point of zero charge. This means that the α-$[S_2W_{18}O_{62}]^{4-/5-}$ process at -0.24 V vs $Fc^{0/+}$ [10] will encounter a very different double layer environment than that of the α-$[S_2W_{18}O_{62}]^{9-/10-}$ one at -2.32 V vs $Fc^{0/+}$ [10]. In this context, studies by Fawcett et al [18] on the impact of tetraalkylammonim electrolytes in dynamic electrochemical studies may be relevant.

The above considerations raise issues concerning how to model the voltammetric reduction of very negatively charged POMs. Historically, most voltammetric (polarographic) studies with this class of compound were undertaken at the dropping mercury electrode [19]. In recent times, use of mercury as an electrode material has been phased out due to toxicity and environmental concerns. In its place, GC often has been the electrode of choice for POM studies, because, like mercury, it provides access to a wide negative potential range. With this electrode material, many more examples of well-defined POM electrochemistry have been reported.[20] However, even if POM processes may have the characteristics of close to reversible or quasi-reversible processes, parameterisation of every process in the α-$[S_2W_{18}O_{62}]^{4-/5-/6-/7-/8-/9-/10-}$ series as a simple one-electron reduction process almost certainly has to be an oversimplification. For example, the α-$[S_2W_{18}O_{62}]^{9-/10-}$ reduction reaction therefore involves highly charged species and occurs at very negative potentials. The process, in addition to electron transfer, is therefore expected to involve changes in ion-pairing and suffer from double layer effects rather than being a simple outer sphere electron transfer

reaction, as commonly assumed. In order to establish the extent to which simple models of electron transfer are adequate for quantitative modelling, we have extended detailed electrode kinetic studies on the α-$[S_2W_{18}O_{62}]^{4-/5-/6-}$ processes to encompass all one-electron transfer processes available at GC, Au and Pt electrodes in acetonitrile containing 0.10 or 0.50 M [*n*-Bu_4N][PF_6] by DC and FTAC voltammetry and other techniques. A progressively increasing level of departure of experimental data from that predicted by the Butler-Volmer model for a simple one-electron transfer process has been found as a consequence of enhanced ion-pairing and electrode material dependent surface interactions associated with the more highly reduced forms. Given that POMs are of widespread interest in electrocatalysis [21-25], supercapacitor[26] and battery development [27-30], enhanced knowledge of subtleties that exist in the POM electrochemistry may assist both fundamental and applied aspects of the field.

2. EXPERIMENTAL SECTION

2.1. Reagents and Solvents. $[n-Bu_4N]_4[\alpha-S_2W_{18}O_{62}]$ was synthesized according to a literature method [31]. Ferrocene (Fc, 98 %, Sigma-Aldrich), Al_2O_3 (diameter = 0.3 μm and 0.05 μm, Buehler), acetonitrile (CH_3CN, 99.9 %, Sigma-Aldrich) and ethanol (99.5 %, Ajax Finechem) were used as obtained from the manufacturer. Tetrabutylammonium hexafluorophosphate ([*n*-Bu_4N][PF_6], 98 %, Sigma-Aldrich) was recrystallized [32] and used as the supporting electrolyte.

2.2. Electrochemical Instrumentation and techniques. Conventional DC voltammetric measurements using stationary GC, Au or Pt working electrodes with Pt wires for both the auxiliary and quasi-reference electrodes were undertaken with a CHI-760E electrochemical workstation. FTAC voltammetric experiments with the same electrodes employed home-built [33] instrumentation using a sine wave perturbation having an amplitude

(ΔE) of 80 mV and a frequency (f) of 8.98 or 26.95 Hz superimposed upon the DC ramp. Frequency domain data in the form of a power spectrum were obtained from the total current–time data by Fourier transformation. Inverse Fourier transformation was applied to the power spectrum using a rectangular window used for band filtering to generate the resolved aperiodic DC and AC harmonic components [34-35].

Steady state rotating disc electrode (RDE) voltammetry of α-$[S_2W_{18}O_{62}]^{4-}$ in CH_3CN (0.50 M [n-Bu_4N][PF_6]) at GC, Au and Pt electrodes was achieved with use of CHI 760E electrochemical workstation at a rotation rate of 52.4 s^{-1} generated by a BAS-M 1005 electrode rotator. In RDE experiments, Pt wire in a glass frit containing 0.50 M [n-Bu_4N][PF_6] in CH_3CN was used as reference electrode and Pt wire as the counter electrode.

All voltammetric experiments were undertaken at 22 ± 2^{o} C. Oxygen was removed from solutions by purging with nitrogen gas for at least 10 min prior to each experiment. eDAC metal (Au and Pt) and GC disc working electrodes were polished with aqueous Al_2O_3 slurry before each voltammetric experiment. Sonication for 10 to 15 seconds was used to remove polishing residue followed by rinsing with water and acetone. Finally, the working electrodes were dried under a flow of nitrogen. The IUPAC recommended $Fc^{0/+}$oxidation process [36] was used to calibrate the potential of the Pt quasi-reference electrode.

The Randles-Sevcik equation [37] (Eq 1) was used to determine the effective area of the macrodisc working electrodes via the DC peak current for oxidation of 1.0 mM Fc to Fc^+ in CH_3CN containing 0.10 M [n-Bu_4N][PF_6] as supporting electrolyte with a known diffusion coefficient (D) of 2.4×10^{-5} cm^2 s^{-1} for Fc [38]. In this equation, I_p, n, C, v, T, R, F and A denote the oxidation peak current, number of electrons transferred in the Fc/Fc^+ process (n = 1), bulk concentration of Fc, scan rate, absolute temperature, universal gas constant, Faraday's constant

and electrode area, respectively. The estimated effective areas of the GC, Pt and Au electrodes determined by this method were 8.0×10^{-3}, 8.0×10^{-3}, and 8.1×10^{-3} cm^2, respectively.

$$I_p = 0.4463nFA(nFDv/RT)^{1/2}C \quad (1)$$

Mass changes accompanying voltammetric experiments at a gold coated quartz crystal electrode (area = 0.205 cm^2, oscillation frequency = 8.0 MHz) were detected by the electrochemical quartz crystal microbalance (EQCM) technique using CHI 400B instrumentation. The reference and auxiliary electrodes for the EQCM experiments and experimental procedures and conditions were the same as in voltammetry.

2.3. Simulations. MECSim (Monash Electro-Chemistry Simulator) software [39] was used to simulate voltammetric data using a model based on a simple one-electron transfer process (Eq 2), where Ox and Red are the oxidised and reduced forms of the POM, with Butler-Volmer theory for electron transfer and mass transport by planner diffusion.

$$Ox + e^- \leftrightarrows Red \ \ (E^0, k^0, \alpha) \quad (2)$$

The parameters E^0 (reversible formal potential), k^0 (heterogeneous charge transfer rate constant) at E^0, α (charge transfer coefficient), D, R_u (uncompensated resistance) and C_{dl} (double layer capacitance) need to be introduced into the simulations in order to mimic experimental data. However, the extensive set of thermodynamically favoured cross redox reactions and ion-pairing reactions are neglected in the simulations. The R_uC_{dl} time constant technique available with the CHI electrochemical workstation was employed to determine R_u. In heuristic forms of data analysis, E^0 was derived from the average of the oxidation (E_p^{ox}) and reduction (E_p^{red}) peak potentials obtained from DC cyclic voltammetric experiments. The diffusion coefficient of α-$[S_2W_{18}O_{62}]^{4-}$ was estimated from the reduction peak current

associated with α-$[S_2W_{18}O_{62}]^{4-/5-}$ reduction process at a GC electrode and use of the Randles-Sevcik relationship [37] (Eq 1). Values determined were 2.9×10^{-6} and 6.3×10^{-6} cm^2 s^{-1}, with 0.50 and 0.10 M [*n*-Bu$_4$N][PF$_6$] as the supporting electrolyte, respectively. A similar relative decrease in diffusion coefficient was also observed for ferrocene on increasing the electrolyte concentration, suggesting that the change in viscosity is the origin.

The value of C_{dl} was estimated at each potential from the fundamental harmonic AC data where faradaic current is absent and use of the potential dependent capacitor model [40].

$$C_{dl}(t) = c_0 + c_1E(t) + c_2E(t)^2 + c_3E(t)^3 + c_4E(t)^4 \qquad (3)$$

In Eq 3, the nonlinearity is defined by c_0, c_1, c_2, c_3, and c_4 and the time dependant potential is denoted by $E(t)$. These coefficients were obtained at each frequency (8.98 or 26.95 Hz).

2.4. Parameterisation. In the initially used heuristic form of parameterisation, comparisons of the AC harmonic components of experimental and simulated data were undertaken visually by the experimenter. E^0 was assumed to be known and values of k^0 and α reported were derived from the experimenter's assessment of the best match of experimental and simulated data. Most aspects of the computer assisted automated data analysis protocol used subsequently is described in detail elsewhere [8]. Briefly, the experimental and simulated data are compared using a high resolution search of parameter space restricted to values near to those estimated heuristically and the least squares (LS) based "best fit" function given in Eq 4 is used to estimate the optimised values of E^0, k^0 and α. The subscript *app* is now applied to the E^0, k^0 and α parameters to designate that a simple electron transfer scheme is used to approximate a more complete square one where ion-pairing is coupled to electron transfer. [41-42] These values are a function of supporting electrolyte concentration. Minimisation of the

influence of non-faradaic current was achieved by analysing only the 2nd to 6th AC harmonic components in the automated form of parameterisation.

$$\mathrm{LS} = \left[1 - \left(\sum_{h=2}^{6} \sqrt{\frac{\sum_{i=1}^{N}\left[\left(f_h^{\exp}(t_i) - f_h^{\mathrm{sim}}(t_i)\right)^2\right]}{\sum_{i=1}^{N} f_h^{\exp}(t_i)^2}}\right)/5\right] \times 100\% \qquad (4)$$

In Eq 4, $f^{\exp}(t_i)$ and $f^{\mathrm{sim}}(t_i)$ symbolize the experimental and simulated functions, respectively and *h* and *N* represent the individual AC harmonic component and number of data points, respectively. The LS percentage fits were calculated independently for each of the α-$[S_2W_{18}O_{62}]^{4-/5-/6-/7-/8-/9-/10-}$ processes using a visually identified potential windowed region where the process of interest occurs. This LS percentage fit includes data derived from both the forward and backward DC potential scan directions for the process of interest. In reference 8 a global LS value encompassing both the $[S_2W_{18}O_{62}]^{4-/5-/6-}$ processes was used.

The tedious heuristic method was used initially to provide a good estimate of the k^0 and α parameters. This dual data analysis strategy facilitates minimisation of the parameter space that needs to be searched in the automated data optimisation method, ensures that physically realistic parameters are reported as the outcome form the data optimisation method and enhances prospects of detection of systematic but subtle discrepancies in experimental and simulated data that are more likely to be detected by visual inspection of data by an experienced experimenter than by relying exclusively on analysis of LS values [8].

3. RESULTS AND DISCUSSION

3.1. DC Cyclic voltammetry of α-$[S_2W_{18}O_{62}]^{4-}$ at GC, Au and Pt Electrodes. DC cyclic voltammograms starting at potentials prior to the initial reduction of α-$[S_2W_{18}O_{62}]^{4-}$ up to the CH_3CN solvent limit were recorded at a scan rate of 0.100 V s^{-1} at GC, Au and Pt electrodes with 0.50 M and 0.10 M [*n*-Bu_4N][PF_6] as the supporting electrolyte (see Figure 2).

The more negative solvent reduction limit at GC allows six reduction steps to be observed that represent consecutive reduction of α-$[S_2W_{18}O_{62}]^{4-}$ to α-$[S_2W_{18}O_{62}]^{5-}$, then to α-$[S_2W_{18}O_{62}]^{6-}$, α-$[S_2W_{18}O_{62}]^{7-}$, α-$[S_2W_{18}O_{62}]^{8-}$, α-$[S_2W_{18}O_{62}]^{9-}$ and finally to α-$[S_2W_{18}O_{62}]^{10-}$ [8, 10]. The lower negative potential limit at the Au electrode restricts reduction to five steps, while the even less negative limit at the Pt electrode allows only three processes to be observed. In contrast with the simpler series of processes seen at GC (six processes with equal peak heights), α-$[S_2W_{18}O_{62}]^{4-}$ voltammetric reduction at Au shows a progressive decease in peak currents. At Pt electrodes, even the third process is barely seen and its shape differs relative to the initial two processes. These observations indicate probable complexity accompanying at least some α-$[S_2W_{18}O_{62}]^{4-}$ reduction processes which means they may not be well-modelled by Butler-Volmer electron transfer theory.

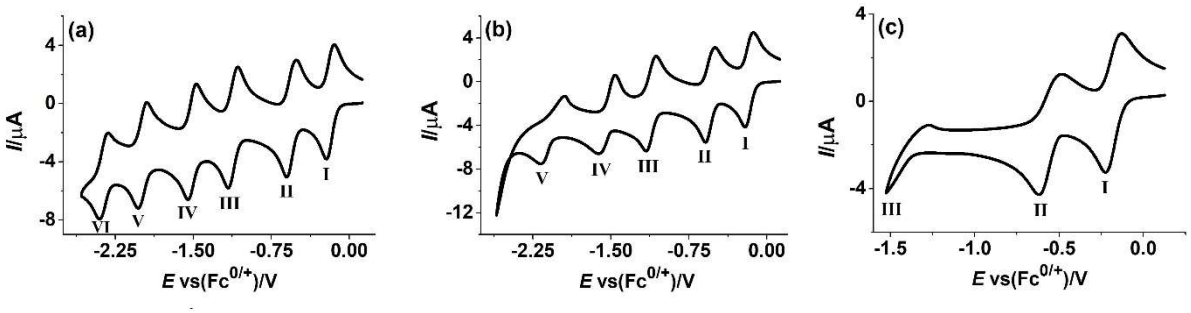

Figure 2. DC cyclic voltammograms obtained at a scan rate of 0.100 V s^{-1} for reduction of 2.5 mM α-$[S_2W_{18}O_{62}]^{4-}$ in CH_3CN (0.10 M [n-Bu_4N][PF_6]) at (a) GC (b) Au and (c) Pt electrodes.

Table 1 summarises the mid-point potential $E_m = (E_P^{ox} + E_P^{red})/2$, which provisionally is equated to E_{app}^0, and the peak-to-peak separation $\Delta E_P = E_P^{ox} - E_P^{red}$ values derived from DC cyclic voltammetry of α-$[S_2W_{18}O_{62}]^{4-}$ in CH_3CN (0.50 and 0.10 M [n-Bu_4N][PF_6] at GC, Au and Pt electrodes. E_{app}^0 values at GC electrode appear at more positive potentials ($E_{app\mathbf{1}}^0 =$ -0.215 V, $E_{app\mathbf{2}}^0 =$ -0.592 V, $E_{app\mathbf{3}}^0 =$ -1.156 V, $E_{app\mathbf{4}}^0 =$ -1.539 V, $E_{app\mathbf{5}}^0 =$ -2.006 V and

E^0_{app6} = -2.344 V) with the higher [*n*-Bu4N][PF6] supporting electrolyte concentration (0.50 M) than with the lower one (0.10 M) (E^0_{app1} = -0.232 V, E^0_{app2} = -0.608 V, E^0_{app3} = -1.178 V, E^0_{app4} = -1.563 V, E^0_{app5} = -2.046 V and E^0_{app6} = -2.409 V). The same scenario also applies for most processes at Au and Pt electrodes, but E^0_{app} values for well-defined processes are only independent of electrode material for processes I to IV (see Table 1). E^0_{app} is a parameter that is assumed to be thermodynamically pinned and hence should be independent of electrode material, so this discrepancy with theoretical predictions based on simple electron transfer reactions is evident. Nevertheless, the positive E^o_{app} shift found with use of 0.50 M [*n*-Bu4N][PF6] instead of 0.10 M [*n*-Bu4N][PF6] supporting electrolyte concentration is consistent with the presence of a stronger ion-pairing impact with the higher electrolyte concentration, as noted in other studies [8, 43].

Table 1. Summary of voltammetric parameters obtained from the reduction of 1.0 mM α-$[S_2W_{18}O_{62}]^{4-}$ in CH_3CN (0.10 and 0.50 M [*n*-Bu4N][PF6]) at a scan rate of 0.100 V s^{-1}.

Electrode	[*n*-Bu4N][PF6] *C* (M)	E^0_{app1}	E^0_{app2}	E^0_{app3}	E^0_{app4}	E^0_{app5}	E^0_{app6}	ΔE_{P1}	ΔE_{P2}	ΔE_{P3}	ΔE_{P4}	ΔE_{P5}	ΔE_{P6}
		V[a] vs $Fc^{0/+}$						V[b]					
GC	0.50	-0.215	-0.592	-1.156	-1.539	-2.006	-2.344	0.060	0.074	0.078	0.078	0.079	0.088
	0.10	-0.232	-0.608	-1.178	-1.563	-2.046	-2.409	0.062	0.075	0.080	0.075	0.087	0.082
Au	0.50	-0.215	-0.593	-1.159	-1.540	-2.025	[c]	0.063	0.077	0.086	0.094	0.150	[c]
	0.10	-0.232	-0.606	-1.174	-1.566	-2.083	[c]	0.068	0.083	0.090	0.100	0.240	[c]
Pt	0.50	-0.218	-0.595	[d]	[c]	[c]	[c]	0.068	0.090	[d]	[c]	[c]	[c]
	0.10	-0.233	-0.606	[d]	[c]	[c]	[c]	0.070	0.100	[d]	[c]	[c]	[c]

[a] Uncertainty in E^0_{app} is $\pm$ 5 mV

[b] Uncertainty in ΔE_P is $\pm$ 2 mV

[c] Overlap with solvent reduction process occurs

[d] Poorly defined process

As previously noted [8] the value $\Delta E_{\mathbf{P1}} = 60$ mV obtained at $v = 0.100$ mV s^{-1} for the α-$[S_2W_{18}O_{62}]^{4-/5-}$ process in CH_3CN (0.50 M [n-Bu_4N][PF_6]) at a GC electrode is close to the theoretically predicted value of 56.4 mV [37] for a reversible one-electron process at 22 °C, signifying that process I can be regarded as reversible on this DC time scale. However, values of this parameter progressively increase upon more extensive reduction ($\Delta E_{\mathbf{P2}} = 0.074$ V, $\Delta E_{\mathbf{P3}} = 0.078$ V, $\Delta E_{\mathbf{P4}} = 0.078$ V, $\Delta E_{\mathbf{P5}} = 0.079$ V and $\Delta E_{\mathbf{P6}} = 0.088$ V). In general, the scenario ($\Delta E_{\mathbf{P1}} < \Delta E_{\mathbf{P2}} \cdots < \Delta E_{\mathbf{Pn}}$) also applies at Au and Pt electrodes, implying that $k^0_{app\mathbf{1}} > k^0_{app\mathbf{2}} \cdots > k^0_{app\mathbf{n}}$ at all electrode materials if the processes truly conform to the Butler-Volmer model for simple quasi-reversible electron transfer reactions. Also noteworthy is the fact that ΔE_{P} values are significantly smaller at the GC electrode than at metal ones ($\Delta E_{\mathbf{P1}} = 0.063$ V, $\Delta E_{\mathbf{P2}} = 0.077$ V, $\Delta E_{\mathbf{P3}} = 0.086$ V, $\Delta E_{\mathbf{P4}} = 0.094$ V and $\Delta E_{\mathbf{P5}} = 0.150$ V at Au and $\Delta E_{\mathbf{P1}} = 0.068$ V and $\Delta E_{\mathbf{P2}} = 0.090$ V at Pt) which according to Butler-Volmer theory implies faster electrode kinetics at the carbon based electrode assuming that the IR_u drop at all electrode materials are comparable or have a negligible impact. The very large ΔE_{P} values at Au for the α-$[S_2W_{18}O_{62}]^{7-/8-}$ and α-$[S_2W_{18}O_{62}]^{8-/9-}$ processes are indicative of very slow electrode kinetics if these are simple one-electron electron transfer reactions.

In principle, studies by DC cyclic voltammetry over a wide range of scan rates could be used to assess to what extent departures from simple one-electron transfer processes occur. However, this is extremely difficult with up to six processes to evaluate with diffusion tails between processes making a major contribution and significant potential dependent charging current contributions at negative potentials. Additionally, maintaining exactly the same electrode state for each scan rate experiment is also problematic. Thus, quantitative studies were attempted using a single FTAC voltammetric experiment and examining the extent to which the Butler-Vomer model is applicable, and extend those undertaken previously with the

α-$[S_2W_{18}O_{62}]^{4-/5-/6-}$ processes [8]. Other advantages of the FTAC voltammetry in quantitative electrode kinetic studies have been surveyed in several reviews [43-46].

3.2. FTAC voltammetric parameterisation of the α-$[S_2W_{18}O_{62}]^{4-/5-/6-/8-/9-/10-}$ reduction processes in CH_3CN (0.50 M [*n*-Bu_4N][PF_6]). The E^0_{app}, k^0_{app} and α_{app} values associated with processes I and II have been established by FTAC voltammetry [8] with results and departures from ideality summarised in the Introduction. Processes I and II along with processes III, IV, V and VI at GC, processes III, IV and V at Au and process III at Pt are now subjected to parameterisation from a single data set collected in one-experiment covering the potential range encompassing processes displayed in Figure 2. Initially, results obtained for reduction of 2.5 mM α-$[S_2W_{18}O_{62}]^{4-}$ in CH_3CN with a high supporting electrolyte concentration (0.50 M [*n*-Bu_4N][PF_6]) are considered.

A summary of the heuristic parametrisation analysis outcome for FTAC voltammetric reduction of 2.5 mM α-$[S_2W_{18}O_{62}]^{4-}$ in CH_3CN (0.50 M [*n*-Bu_4N][PF_6]) over the potential range of 0.15 V to −2.525 V for GC (six processes) and Au (five processes) and 0.15 V to −1.375 V for Pt electrodes (three processes) is provided in Table 2. A comparison of experimental and simulated FTAC voltammetric data based on parameters provided in this Table are displayed in Figures 3 and S1 for GC, and Figures S2 and S3 for Au and Figure S4 for the Pt electrode.

As noted in reference [8], only lower limits of $k^0_{app\mathbf{1}}$ could be determined at GC at the low frequency of 8.98 Hz (Figure 3) by the FTAC voltammetric method as this response lies at the reversible limit within experimental uncertainty. Thus, only the thermodynamic parameter $E^0_{app\mathbf{1}}$ is needed to define this FTAC voltammetry. On the other hand, subsequent processes are significantly slower and even at this low frequency can be well-simulated with

electrode kinetic parameters that lie well below the reversible limit. However, the heuristically estimated values of $k^0_{app\mathbf{1}}$ and $\alpha_{app\mathbf{1}}$ reported at the higher frequency (shorter time scale) of 26.95 Hz for the first process are considered reliable as they were derived from the experimenter determined "best fit" simulation undertaken with kinetic parameters consistent with a quasi-reversible process (Figure S1g).

Figures 3 and S1 show the FTAC voltammetric comparison between simulated and experimental data at GC electrode as assessed heuristically. The experimenter in this exercise, as in previous work [8] decided to strive for an almost perfect fit for AC harmonic reduction data (negative DC potential scan direction). However, this meant that for processes III, IV, V and VI, the experimental oxidative component obtained on the reverse positive DC scan direction displayed a level of discrepancy which increased progressively the higher the order of the AC harmonic. Consistent with this outcome, experiment-theory comparisons of the aperiodic DC component display progressively poorer agreement beyond processes I and II. Effectively, in this data analysis approach, the experimenter has biased the parameterisation to the reduction components of the AC harmonics to give $k^0_{app\mathbf{1}} = \geq 0.10$, $k^0_{app\mathbf{2}} = 0.080$, $k^0_{app\mathbf{3}} = 0.053$, $k^0_{app\mathbf{4}} = 0.041$, $k^0_{app\mathbf{5}} = 0.012$ and $k^0_{app\mathbf{6}} = 0.002$ cm s^{-1} at 8.98 Hz and $k^0_{app\mathbf{1}} = 0.10$, $k^0_{app\mathbf{2}} = 0.084$, $k^0_{app\mathbf{3}} = 0.057$, $k^0_{app\mathbf{4}} = 0.045$, $k^0_{app\mathbf{5}} = 0.014$ and $k^0_{app\mathbf{6}} = 0.002$ cm s^{-1} at 26.95 Hz. However, a major virtue of this strategy is that the electrode kinetics for all processes are independent of frequency as required by the Butler-Volmer model. Kinetic values for the 6th process were only determined from the 1st to 3rd harmonic AC components, rather than from the 1st to 6th harmonics used for processes I to V, as the AC current magnitude in higher harmonics is very small. The experimenter could of course have chosen alternative heuristic data analysis strategies and tried to fit data to the average of the reduction and oxidation harmonic data, but experience [8] suggested the approach taken is the most reasonable one to be

adopted. However, this highlights the subjectivity of the heuristic method of data analysis and the likelihood of experimenter dependent outcomes.

Close inspection of Figures 3 and S1, reveals an inequality in the reduction and oxidation component peak current magnitudes for the α- $[S_2W_{18}O_{62}]^{4-/5-}$ and α-$[S_2W_{18}O_{62}]^{5-/6-}$ processes. Furthermore, this form of asymmetry does not exist when these processes I and II were examined individually by FTAC voltammetry [8] rather than when the potential was switched after all six reduction steps had been completed. This represents another subtle departure from ideality for the series of quasi-reversible process detected via visual inspection of the voltammograms as required in the heuristic form of data analysis and implies that complexity at a GC electrode is introduced at potentials more negative than process II. Furthermore, it can be concluded that the origin of this modelling imperfection is unlikely to be accommodated fully by inclusion of ion-pairing in combination with very sluggish electrode kinetics which was proposed as a plausible explanation for the asymmetry in reduction and oxidation components found with the α-$[S_2W_{18}O_{62}]^{5-/6-}$ process at a Pt electrode [8].

Table 2. Thermodynamic and electrode kinetic parameters[a] derived from heuristic and automated computer based comparison of simulated and experimental FTAC voltammetric data at GC, Au and Pt electrodes for the reduction of 2.5 mM α-$[S_2W_{18}O_{62}]^{4-}$ in CH_3CN (0.50 M [*n*-Bu_4N][PF_6]).

(a) Reversible potentials:

Electrode	f(Hz)	R_u (Ω)[b]	Optimisation method		E^0_{app1}	E^0_{app2}	E^0_{app3}	E^0_{app4}	E^0_{app5}	E^0_{app6}
					V vs $Fc^{0/+}$					
GC	8.98	225	Heuristic		-0.215	-0.592	-1.156	-1.539	-2.006	-2.344
			Automated	Range	-0.220 to -0.210	-0.596 to -0.585	-1.165 to -1.148	-1.543 to -1.531	-2.014 to -2.003	-2.354 to -2.337
				Est.	-0.212	-0.589	-1.154	-1.537	-2.004	-2.349
	26.95	200	Heuristic		-0.215	-0.592	-1.156	-1.539	-2.006	-2.344
			Automated	Range	-0.220 to -0.210	-0.599 to -0.585	-1.163 to -1.148	-1.544 to -1.530	-2.013 to -2.003	-2.354 to -2.337
				Est.	-0.212	-0.588	-1.153	-1.535	-2.008	-2.345
Au	8.98	180	Heuristic		-0.215	-0.593	-1.159	-1.540	-2.025	[c]
			Automated	Range	-0.224 to -0.210	-0.601 to -0.587	-1.164 to -1.151	-1.548 to -1.530	-2.040 to -2.015	--
				Est.	-0.212	-0.589	-1.158	-1.538	-2.030	--
	26.95	180	Heuristic		-0.215	-0.593	-1.159	-1.540	-2.025	[c]
			Automated	Range	-0.222 to -0.207	-0.601 to -0.585	-1.163 to -1.152	-1.550 to -1.532	-2.035 to -2.015	--
				Est.	-0.211	-0.588	-1.155	-1.5387	-2.0301	--
Pt	8.98	200	Heuristic		-0.218	-0.593	[d]	[c]	[c]	[c]
			Automated	Range	-0.220 to -0.214	-0.596 to -0.589	--	--	--	--
				Est.	-0.218	-0.591	--	--	--	--
	26.95	200	Heuristic		-0.218	-0.593	[d]	[c]	[c]	[c]
			Automated	Range	-0.220 to -0.214	-0.599 to -0.592	--	--	--	--
				Est.	-0.219	-0.592	--	--	--	--

[a] Other Parameters used in the simulations are: $A_{GC} = 8.0 \times 10^{-3}$ cm^2, $A_{Au} = 8.1 \times 10^{-3}$ cm^2, $A_{Pt} = 8.0 \times 10^{-3}$ cm^2, $\Delta E = 80$ mV, $D = 2.9 \times 10^{-6}$ cm^2 s^{-1}, $T = 295$ K, $v_{GC} = 0.099$ V s^{-1}, $v_{Au} = 0.100$ V s^{-1} and $v_{Pt} = 0.057$ V s^{-1}, $f_{GC,Au\ and\ Pt} = 8.98$ and 26.95 Hz.

[b] small differences due to slight variability in electrode arrangement [c] process is not observed due to less negative potential limit for solvent reduction. [d] poorly defined.

(b) Heterogeneous charge transfer kinetics:

Electrode	f(Hz)	Optimisation method		k^0_{app1}	k^0_{app2}	k^0_{app3}	k^0_{app4}	k^0_{app5}	k^0_{app6}
				cm s^{-1}					
GC	8.98	Heuristic		≥0.10	0.080[a]	0.053[a]	0.041	0.012	0.002[b]
		Automated	Range	0.070 to 0.140	0.045 to 0.090	0.035 to 0.065	0.030 to 0.055	0.008 to 0.014	0.0005 to 0.0050
			Est.	0.10[c]	0.064[d]	0.042[d]	0.047	0.013	0.002[b]
	26.95	Heuristic		0.10	0.084[a]	0.057[a]	0.045	0.014	0.002[b]
		Automated	Range	0.070 to 0.140	0.045 to 0.090	0.040 to 0.070	0.030 to 0.055	0.009 to 0.019	0.0005 to 0.0050
			Est.	0.099	0.060[d]	0.045[d]	0.045	0.014	0.0017[b]
Au	8.98	Heuristic		0.053	0.039[a]	0.017	0.002[b]	0.0004[b]	[e]
		Automated	Range	0.035 to 0.065	0.025 to 0.045	0.009 to 0.025	0.0006 to 0.005	0.0001 to 0.0008	--
			Est.	0.051	0.028[d]	0.013	0.0042[b]	0.0003[b]	--
	26.95	Heuristic		0.054	0.039[a]	0.015	0.002[b]	0.0004[b]	[e]
		Automated	Range	0.035 to 0.065	0.025 to 0.045	0.009 to 0.025	0.0006 to 0.005	0.0001 to 0.0008	--
			Est.	0.055	0.031[d]	0.015	0.0044[b]	0.0005[b]	--
Pt	8.98	Heuristic		0.039	0.012[a]	0.00001[f]	[e]	[e]	[e]
		Automated	Range	0.025 to 0.045	0.004 to 0.014	--	--	--	--
			Est.	0.036	0.009[d]	--	--	--	--
	26.95	Heuristic		0.037	0.011[a]	0.00001[f]	[e]	[e]	[e]
		Automated	Range	0.033 to 0.042	0.004 to 0.014	--	--	--	--
			Est.	0.038	0.008[d]	--	--	--	--

[a] determined only from reduction component of data. [b] estimated from 1st to 3rd harmonic components. [c] close to reversible limit so uncertainty substantial. [d] derived from use of all data even though current magnitude asymmetry is present in reduction and oxidation components. See text for details. [e] process is not observed due to less negative potential limit for solvent reduction. [f] poorly defined.

(c) Charge transfer coefficients:

Electrode	f (Hz)	Optimisation method		α_{app1}	α_{app2}	α_{app3}	α_{app4}	α_{app5}	α_{app6}
GC	8.98	Heuristic		[a]	0.60	0.60	0.55	0.53	0.50[b]
		Automated	Range	0.40 to 0.70	0.40 to 0.70	0.40 to 0.70	0.40 to 0.70	0.40 to 0.70	0.40 to 0.70
			Est.	0.58[c]	0.48[d]	0.54[d]	0.41[d]	0.51	0.48[b]
	26.95	Heuristic		0.60	0.60	0.60	0.55	0.53	0.50[b]
		Automated	Range	0.40 to 0.70	0.40 to 0.70	0.40 to 0.70	0.40 to 0.70	0.40 to 0.70	0.40 to 0.70
			Est.	0.49[d]	0.59	0.57[d]	0.51[d]	0.51	0.51[b]
Au	8.98	Heuristic		0.60	0.60	0.47	0.50[b]	0.50[b]	[e]
		Automated	Range	0.40 to 0.70	0.40 to 0.70	0.40 to 0.70	0.40 to 0.70	0.40 to 0.70	--
			Est.	0.58	0.60	0.41[d]	0.42[b]	0.60[b]	[e]
	26.95	Heuristic		0.60	0.60	0.47	0.50[b]	0.50[b]	[e]
		Automated	Range	0.40 to 0.70	0.40 to 0.70	0.40 to 0.70	0.40 to 0.70	0.40 to 0.70	--
			Est.	0.64	0.64	0.47	0.41[b]	0.47[b]	[e]
Pt	8.98	Heuristic		0.57	0.50	0.50[f]	[e]	[e]	[e]
		Automated	Range	0.40 to 0.70	0.44 to 0.60	--	--	--	--
			Est.	0.57	0.53	--	[e]	[e]	[e]
	26.95	Heuristic		0.57	0.50	0.50[f]	[e]	[e]	[e]
		Automated	Range	0.50 to 0.67	0.44 to 0.65	--	--	--	--
			Est.	0.56	0.52	--	[e]	[e]	[e]

[a] too close to reversible limit to be determined. [b] estimated from 1st to 3rd harmonic components. [c] near reversible limit so uncertainty substantial [d] all data used in analysis. [e] process is not observed due to less negative potential for solvent reduction [f] poorly defined.

Table 3. Least square (LS) values obtained from the automated computer-based comparison of simulated and experimental FTAC voltammetric data for the reduction of 2.5 mM α-$[S_2W_{18}O_{62}]^{4-}$ in CH_3CN.

Electrode	f (Hz)	LS (%) 0.50 M [n-Bu_4N][PF_6]						LS (%) 0.10 M [n-Bu_4N][PF_6]					
		I	II	III	IV	V	VI	I	II	III	IV	V	VI
GC	8.98	86	74	85	71	85	70	90	91	87	90	89	82
	26.95	89	84	81	82	84	56	82	91	91	87	89	85
Au	8.98	85	81	78	53	41		88	85	80	67	44	
	26.95	80	77	76	51	37		85	84	74	70	48	
Pt	8.98	91	58					93	61				
	26.95	85	55					89	60				

All heuristically estimated k^0_{app} and α_{app} values at Au and Pt electrodes are considered to be reliable in the context that they lie significantly below the reversible limit, even with the lower frequency (f = 8.98 Hz). Thus, significantly slower electrode kinetics apply for all processes at these metal electrodes than at GC. Again, if the data analysis in the heuristic approach is biased to obtain an excellent fit to the reduction component of the data set, with discrepancies in the oxidation component, then parameterisation of data obtained from the Au electrode gives $k^0_{app\mathbf{1}} = 0.053$, $k^0_{app\mathbf{2}} = 0.039$ cm s^{-1}, $k^0_{app\mathbf{3}} = 0.017$, $k^0_{app\mathbf{4}} = 0.002$ and $k^0_{app\mathbf{5}} = 0.0004$ cm s^{-1} at 8.98 Hz and $k^0_{app\mathbf{1}} = 0.054$, $k^0_{app\mathbf{2}} = 0.039$ cm s^{-1}, $k^0_{app\mathbf{3}} = 0.015$, $k^0_{app\mathbf{4}} = 0.002$ and $k^0_{app\mathbf{5}} = 0.0004$ cm s^{-1} at 26.95 Hz.

Consistent with the conclusion of slower kinetics at metal electrodes, it is noted that parameter estimations for the 4th and 5th processes at the gold electrode were based solely on a comparison of 1st to 3rd AC harmonic components of experimental and simulated data versus 1st to 6th at GC electrode, because the current magnitudes of higher harmonics are too small and the 6th harmonic is not detectable above background noise. Significant asymmetry also appears in the higher harmonic AC component data at the Au electrode as at GC. The level of

agreement between simulated and experimental data obtained at the Au electrode is displayed in Figures S2 and S3.

Electrode kinetics at the Pt electrode ($k^0_{app\mathbf{1}} = 0.039$, $k^0_{app\mathbf{2}} = 0.012$ and $k^0_{app3} = 0.00001$ cm s^{-1} at 8.098 Hz and $k^0_{app\mathbf{1}} = 0.037$, $k^0_{app\mathbf{2}} = 0.011$ and $k^0_{app3} = 0.00001$ cm s^{-1} at 26.95 Hz) (see Figure S4) are even slower than at Au electrodes. k^0_{app} was again estimated in the heuristic approach from the reduction component of the AC harmonics due to asymmetry in current reduction and oxidation components as noted in the earlier report [8].

With the computer assisted data optimisation approach, theory-experiment comparisons were confined to the 2nd to 6th harmonics where the influence of background current is negligible. Unlike the heuristic method, parameters were now derived from use of all data, so parameter values may differ from those estimated by heuristic analysis that solely utilise the reduction component of the data set. Nevertheless, to save substantial computational time in estimation of up to 18 parameters, values obtained heuristically were still used to minimise range of the parameter space search needed in the automated data optimisation method. Significantly, implementation of this strategy meant that up to six sets of E^0_{app} as well as six sets of k^0_{app} and α_{app} parameter values or 18 parameter values as applies at a GC electrode can now all be conveniently and efficiently derived in one data optimisation exercise to give the results summarised in Table 2.

Computer data optimisation methods lead to a best fit outcome according to the model used to mimic experimental data. LS values, which provide a measure of the agreement between modelled and experimental data, are provided in Table 3 for each of the processes parameterised by data optimisation at GC, Au and Pt electrodes. These data confirm that with 0.50 M [*n*-Bu$_4$N][PF$_6$] as the supporting electrolyte, agreement for process I is highest with LS

values at about 90% at all electrodes and then progressively decreases to less than 50% in some cases as the extent of reduction increases. However, agreement at GC is always superior to that at Au and Pt electrodes. It is noteworthy that an experienced experimentalist is able to recognise systematic non-ideality in patterns of behaviour heuristically as found in this study and suggest models that might improve the agreement. In contrast data optimisation solely giving LS values as a number is not as helpful in this sense. Computer supported data optimisation as applied above, provides significantly less "intelligence" that available with the heuristic method where an experimenter can use their discretion and judiciously modify the data analysis strategy as was done in this case. To compete with the ability of the experimenter, data optimisation methods would need to be supported by machine learning [47-48].

While E^0_{app} Values estimated for all processes are essentially independent of the parameterisation method k^0_{app} and α_{app} values differ. As expected, the data optimisation method essentially "averages" outcomes of the reduction and oxidation data sets to produce the "best fit" to the full data set whereas in the heuristic form of analysis, data analysis is deliberately biased to achieving the "best fit" to the reduction component of the data set. The outcome is that automated data optimisation method accommodates the asymmetry by fitting theory to a lower average current than for the heuristic method, and consequently produces lower estimates of k^0_{app} and different values of α_{app} as shown in data presented in Table 2. However, the estimated k^0_{app} values maintain close to frequency independence. For example, at the GC electrode, $k^0_{app\mathbf{2}} = 0.064$ and $k^0_{app\mathbf{3}} = 0.042$ cm s^{-1} with a frequency of 8.98 Hz, versus $k^0_{app\mathbf{2}} = 0.060$ and $k^0_{app\mathbf{3}} = 0.045$ cm s^{-1} at 26.95 Hz. Parallel observations are made with the modelling with Au and Pt electrodes. Attempts to mimic the asymmetry found in experimental data in the automated parametrization exercise, but not in the heuristic approach also lead to data analysis dependent α_{app} values. For example, at the GC electrode, $\alpha_{app\mathbf{2}} =$

0.48, $\alpha_{app3} = 0.54$ at 8.98 Hz using automated data optimisation versus $\alpha_{app2} = 0.60$, $\alpha_{app3} = 0.60$ obtained heuristically.

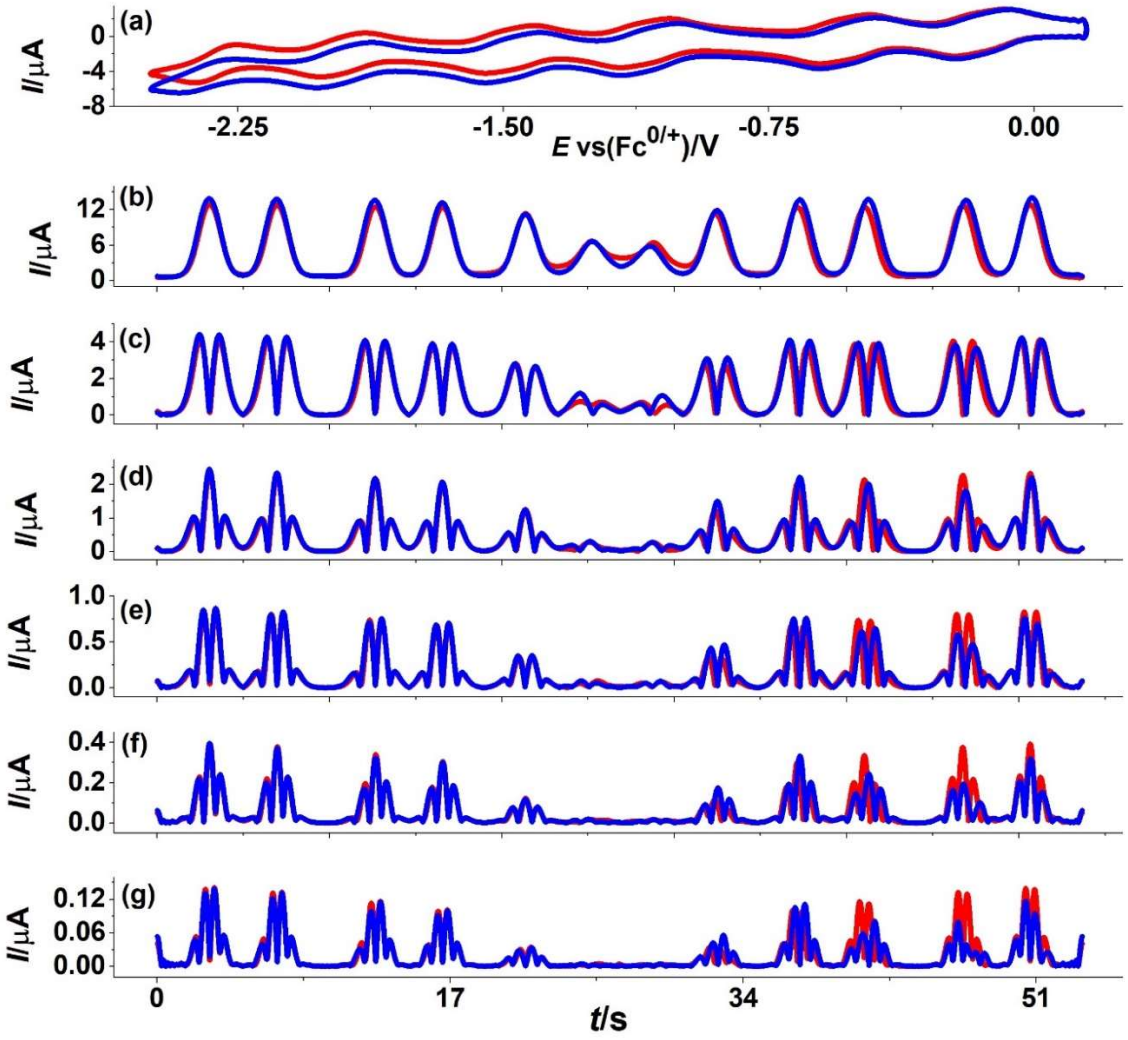

Figure 3. Heuristic comparison of simulated (red line) and experimental (blue line) FTAC voltammetric data for the α-$[S_2W_{18}O_{62}]^{4-/5-/6-/7-/8-/9-/10-}$ processes obtained with $\Delta E =$ 80 mV, $f =$ 8.98 Hz and $v =$ 0.099 V s^{-1} derived from reduction of 2.5 mM α-$[S_2W_{18}O_{62}]^{4-}$ in CH_3CN containing 0.50 M [n-Bu_4N][PF_6] at GC electrode. (a) DC component, (b-g) 1st to 6th harmonic components. Other parameters given in Table 2 and text.

3.3. FTAC voltammetric parameterisation of the α-$[S_2W_{18}O_{62}]^{4-/5-/6-/8-/9-/10-}$ reduction processes in CH_3CN (0.10 M [*n*-Bu_4N][PF_6]). Parameterisation using a lower concentration (0.10 M) of [*n*-Bu_4N][PF_6] supporting electrolyte also was used to investigate the impact of a lower level of ion-pairing predicted to be present relative to the 0.50 M electrolyte studies described above.

Table 4. Electrode kinetic parameters[a] derived from heuristic and computer based automated comparison o voltammetric data at GC, Au and Pt electrodes for the reduction of 2.5 mM α-$[S_2W_{18}O_{62}]^{4-}$ in CH_3CN conta

(a) Reversible potential:

Electrode	f (Hz)	R_u[b]	Optimisation method		E^0_{app1}	E^0_{app2}	E^0_{app3}	E^0_{app4}
					V vs $Fc^{0/+}$			
GC	8.98	625	Heuristic		-0.232	-0.608	-1.178	-1.563
			Automated	Range	-0.238 to -0.226	-0.614 to -0.600	-1.182 to -1.170	-1.567 to -1.554
				Est.	-0.233	-0.604	-1.172 1	-1.557
	26.95	580	Heuristic		-0.232	-0.608	-1.178	-1.563
			Automated	Range	-0.236 to -0.224	-0.612 to -0.599	-1.184 to -1.172	-1.569 to -1.556
				Est.	-0.230	-0.606	-1.181	-1.561
Au	8.98	600	Heuristic		-0.232	-0.606	-1.174	-1.566
			Automated	Range	-0.239 to -0.225	-0.612 to -0.599	-1.180 to -1.168	-1.570 to -1.548
				Est.	-0.232	-0.601	-1.174	-1.562
	26.95	580	Heuristic		-0.232	-0.606	-1.174	-1.566
			Automated	Range	-0.236 to -0.223	-0.612 to -0.599	-1.180 to -1.168	-1.570 to -1.550
				Est.	-0.230	-0.603	-1.173	-1.570
Pt	8.98	602	Heuristic		-0.233	-0.606	[d]	[c]
			Automated	Range	-0.238 to -0.228	-0.612 to -0.600	--	--
				Est.	-0.232	-0.604	--	--
	26.95	552	Heuristic		-0.233	-0.606	[d]	[c]
			Automated	Range	-0.238 to -0.228	-0.612 to -0.600	--	--
				Est.	-0.231	-0.605	--	--

[a] Other Parameters used in the simulations are: $A_{GC} = 8.0 \times 10^{-3}$ cm^2, $A_{Au} = 8.1 \times 10^{-3}$ cm^2, $A_{Pt} = 8.0 \times 10^{-3}$ cm^2, $\Delta E =$ K, $v_{GC} = 0.099$ V s^{-1}, $v_{Au} = 0.100$ V s^{-1} and $v_{Pt} = 0.057$ V s^{-1}, $f_{GC,Au\ and\ Pt} = 8.98$ and 26.95 Hz.

[b] small differences due to slight variability in electrode arrangement [c] process is not observed due to overlap with solve

(b) Heterogeneous charge transfer kinetics:

Electrode	f (Hz)	Optimisation method		k^0_{app1}	k^0_{app2}	k^0_{app3}	k^0_{app4}	
				cm s^{-1}				
GC	8.98	Heuristic		≥0.19	0.14[a]	0.058[a]	0.055	
		Automated	Range	0.12 to 0.25	0.090 to 0.165	0.035 to 0.065	0.043 to 0.068	0.02
			Est.	0.18[b]	0.11[c]	0.046[c]	0.062	
	26.95	Heuristic		0.18[a]	0.13[a]	0.060	0.056	
		Automated	Range	0.07 to 0.14	0.045 to 0.090	0.040 to 0.070	0.030 to 0.055	0.00
			Est.	0.16[c]	0.11[c]	0.062	0.062	
Au	8.98	Heuristic		0.11	0.11[a]	0.024	0.0018[d]	0
		Automated	Range	0.07 to 0.16	0.07 to 0.016	0.016 to 0.030	0.0007 to 0.005	0.000
			Est.	0.119	0.087[c]	0.026	0.0045[d]	0
	26.95	Heuristic		0.11	0.11	0.020[a]	0.0018[d]	0
		Automated	Range	0.035 to 0.065	0.025 to 0.045	0.009 to 0.025	0.0007 to 0.005	0.000
			Est.	0.119	0.10	0.029[c]	0.0047[d]	0.
Pt	8.98	Heuristic		0.077	0.022[a]	0.00001[f]	[e]	
		Automated	Range	0.060 to 0.095	0.012 to 0.030	--	--	
			Est.	0.075	0.017[c]	--	--	
	26.95	Heuristic		0.075	0.021[a]	0.00001[f]	[e]	
		Automated	Range	0.060 to 0.095	0.012 to 0.030	--	--	
			Est.	0.072	0.016[c]	--	--	

[a] determined from reduction component of data only [b] near reversible limit so uncertainty substantial [c] derived from us
present in reduction and oxidation components [d] estimated from 1st to 3rd harmonic components [e] process is not observe
process. [f] poorly defined.

(c) Charge transfer coefficient:

Electrode	f (Hz)	Optimisation method		α_{app1}	α_{app2}	α_{app3}	α_{app4}	α_{app5}	α_{app6}
GC	8.98	Heuristic		[a]	0.60	0.70	0.64	0.60	0.50
		Automated	Range	0.40 to 0.70	0.40 to 0.70	0.40 to 0.70	0.40 to 0.70	0.40 to 0.70	0.40 to 0.70
			Est.	0.64[b]	0.55	0.60[c]	0.63	0.57	0.57[c]
	26.95	Heuristic		0.55	0.58	0.60	0.60	0.60	0.50
		Automated	Range	0.40 to 0.70	0.40 to 0.70	0.40 to 0.70	0.40 to 0.70	0.40 to 0.70	0.40 to 0.70
			Est.	0.67[c]	0.51[c]	0.49[c]	0.53[c]	0.43[c]	0.53
Au	8.98	Heuristic		0.60	0.60	0.55	0.50[d]	0.50[d]	[e]
		Automated	Range	0.40 to 0.70	0.40 to 0.70	0.40 to 0.70	0.40 to 0.70	0.40 to 0.70	--
			Est.	0.57	0.65	0.57	0.42[d]	0.60[d]	--
	26.95	Heuristic		0.60	0.60	0.52	0.50[d]	0.50[d]	[e]
		Automated	Range	0.40 to 0.70	0.40 to 0.70	0.40 to 0.70	0.40 to 0.70	0.40 to 0.70	--
			Est.	0.64	0.60	0.59	0.41[d]	0.45[d]	--
Pt	8.98	Heuristic		0.57	0.50	0.50[f]	[e]	[e]	[e]
		Automated	Range	0.40 to 0.70	0.44 to 0.60	--	--	--	--
			Est.	0.60	0.55[c]	--	--	--	--
	26.95	Heuristic		0.58	0.50	0.50[f]	[e]	[e]	[e]
		Automated	Range	0.50 to 0.67	0.44 to 0.65	--	--	--	--
			Est.	0.56	0.52	--	--	--	--

[a] too close to reversible limit to be determined. [b] near reversible limit so uncertainty substantial. [c] all data used. [d] estimated from analysis of 1st to 3rd harmonic components. [e] process is not observed due to overlap with solvent reduction process. [f] poorly defined.

Table 4 summarises the thermodynamic and electrode kinetic parameters obtained using the same heuristic and computer supported data optimisation protocols applied above with 0.50 M [*n*-Bu$_4$N][PF$_6$] as the supporting electrolyte, but now with 0.10 M [*n*-Bu$_4$N][PF$_6$]. Clearly, as expected and as revealed from comparison of data in Tables 2 and 4, the uncompensated resistance has increased with the use of the lower 0.10 M supporting electrolyte concentration. There is also a negative shift in E^0_{app}: with 0.10 M [*n*-Bu$_4$N][PF$_6$], E^0_{app1} = -0.232, E^0_{app2} = -0.608, E^0_{app3} = -1.178, E^0_{app4} = -1.563 V, E^0_{app5} = -2.046 and E^0_{app6} = -2.409 V vs $Fc^{0/+}$ versus E^0_{app1} = -0.215, E^0_{app2} = -0.592, E^0_{app3} = -1.156, E^0_{app4} = -1.539, E^0_{app5} = -2.006 and E^0_{app6} = -2.344 V vs $Fc^{0/+}$ using 0.50 M [*n*-Bu$_4$N][PF$_6$]). Agreement between simulated and experimental data that correspond to each reduction process also is improved as demonstrated by higher LS values (see Table 3) from automated data optimisation results and visual inspection of heuristic comparison of experimental and simulated data shown Figure 3 versus Figure 4 at the GC electrode. The values of k^0_{app1}, k^0_{app2}, k^0_{app3}, k^0_{app4}, k^0_{app5} and k^0_{app6} generally increase on use of the lower electrolyte concentration. For example, k^0_{app} values of ≥0.10, 0.080, 0.053, 0.041, 0.012 and 0.002 cm s^{-1} with 0.50 M electrolyte present increase to ≥0.19, 0.14, 0.058, 0.055, 0.031 and 0.02 cm s^{-1} for the six processes detected at the GC electrode according to heuristically derived data at 8.98 Hz (see Tables 2 and 4). This enhanced electron transfer kinetics could be at least partially attributed to the decrease in solvent viscosity at lower electrolyte concentration [49].

Analogous electrolyte dependence is found at Au (Figures S6 and S7) and Pt electrodes (Figure S8) to that at GC. For example, according the heuristic method of data analysis, the k^0_{app1}, k^0_{app2} and k^0_{app3} values increase from 0.053, 0.039 and 0.017 cm s^{-1} to 0.11, 0.11 and 0.024 cm s^{-1} respectively at the Au electrode using analysis of data collected at 8.98 Hz on decreasing the supporting electrolyte concentration from 0.50 M to 0.10 M. However, it should

be noted that the 4th and 5th processes at this electrode are very slow and display pronounced departures from Butler-Volmer prediction for a simple electron transfer process at both concentrations of [*n*-Bu_4N][PF_6] in both FTAC and DC voltammetry (Figures S2, S3, S6 and S7).

While decreased, some residual current magnitude asymmetry not accommodated in the modelling remains in the reduction-oxidation components of the higher order AC harmonics (see Figures 4, S5, S6, S7 and S8) with 0.10 M electrolyte concentration. This leads to smaller but nevertheless still detectable systematic differences in electrode kinetic evaluations obtained by use of heuristic and automated data optimisation methods.

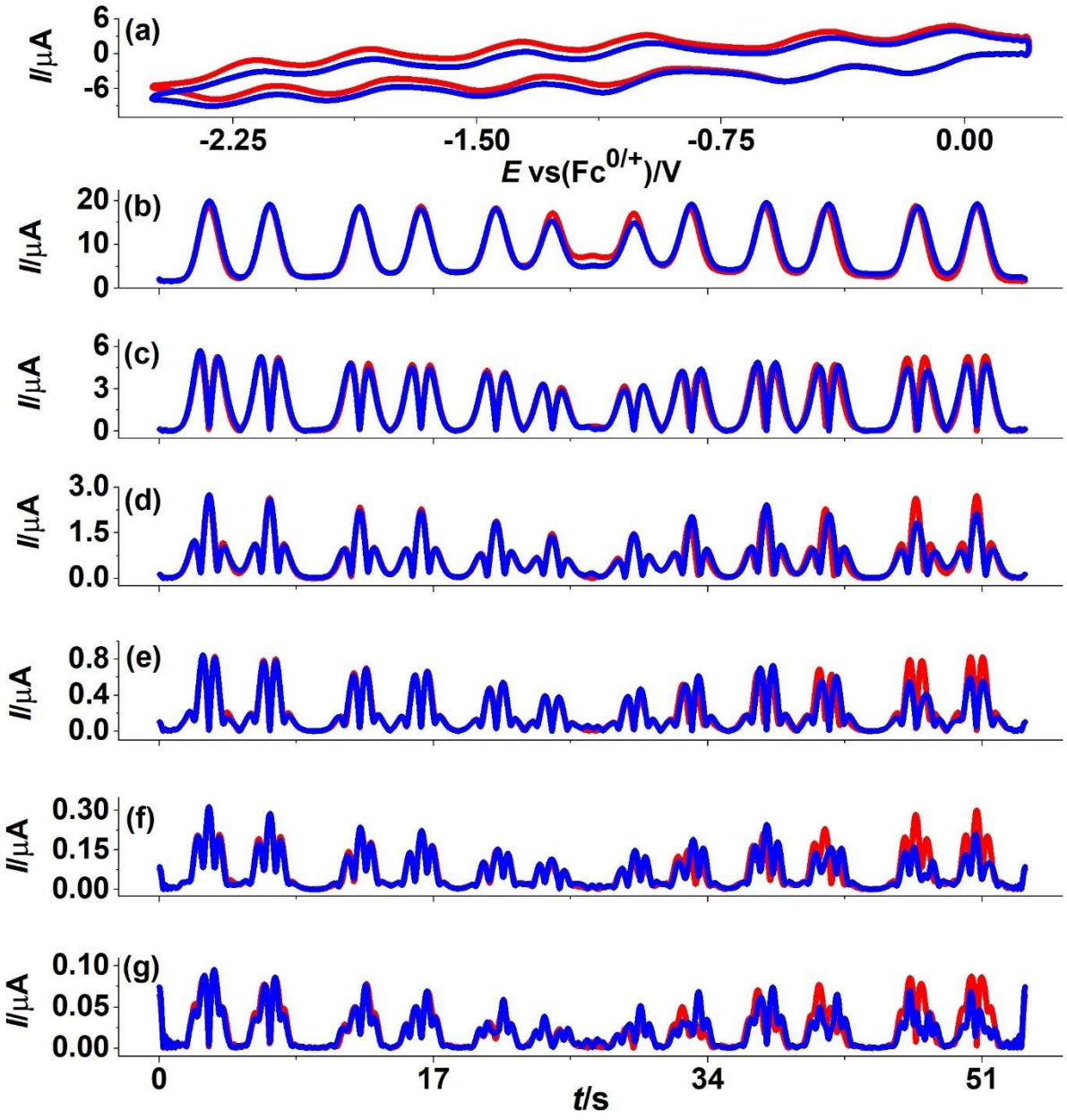

Figure 4. Heuristic comparison of simulated (red line) and experimental (blue line) FTAC voltammetric data for the α-$[S_2W_{18}O_{62}]^{4-/5-/6-/7-/8-/9-/10-}$ processes obtained with ΔE = 80 mV, f = 8.98 Hz and v = 0.099 V s^{-1} derived from reduction of 2.5 mM α-$[S_2W_{18}O_{62}]^{4-}$ in CH_3CN containing 0.10 M [n-Bu_4N][PF_6] at GC electrode. (a) DC component, (b-g) 1st to 6th harmonic components. Other parameters given in Table 4 and text.

3.4. Origin of departures from the Butler-Volmer model of electron transfer. There are a series of non-idealities that emerge from modelling the electrode kinetics of up to six

well-resolved processes when reduction of α-$[S_2W_{18}O_{62}]^{4-}$ occurs in CH_3CN containing [*n*-Bu_4N][PF_6] as the supporting electrolyte. Indeed, as summarised in points (a) to (e) below, this wide potential reduction range feature involving an overall charge change from 4^- to 10^- is very informative in understanding electrode and electrolyte dependent nuances in modelling the voltammetry with the Butler-Volmer relationship.

(a) The heterogeneous charge transfer rate constant decreases as each electron transfer process is encountered at a progressively more negative potentials ($k^0_{app\mathbf{1}} > k^0_{app\mathbf{2}} > k^0_{app\mathbf{3}} > k^0_{app\mathbf{4}} > k^0_{app\mathbf{5}} > k^0_{app\mathbf{6}}$). Thus, the $[S_2W_{18}O_{62}]^{4-/5-}$ process is reversible or close to reversible while the α-$[S_2W_{18}O_{62}]^{9-/10}$ process is kinetically very sluggish.

(b) Non-conformance to the Butler-Volmer model progressively increases with respect to the process order as in (a). Thus, processes I and II that are close to reversible complying well with predictions of this model, whereas slow processes III to VI that occur at more negative potentials display a significant level of non-ideality. However, interestingly while the α-$[S_2W_{18}O_{62}]^{4-/5-/6-}$ processes conform very well with the Butler-Volmer model when the potential is switched immediately after the α-$[S_2W_{18}O_{62}]^{5-/6-}$ process, the level of agreement decreases when the potential is switched at very negative potentials after the α-$[S_2W_{18}O_{62}]^{9-/10-}$process.

(c) k^0_{app} increases as the [*n*-Bu_4N][PF_6] electrolyte concentration is decreased from 0.50 to 0.10 M.

(d) k^0_{app} values are highest at GC electrodes, and smallest at Pt, with values at Au being intermediate between GC and Pt. The level of conformance with the Butler-Volmer model also follows the order GC > Au > Pt.

(e) The non-conformance of data with the Butler-Volmer model is translated into apparently data analysis method dependent values of k^0_{app}.

In principle, the fact that the level of non-conformance to the Butler-Volmer model for increases significantly when the voltammetric experiment includes the potential region where $[S_2W_{18}O_{62}]^{7-}$ and further reduced forms are generated suggests that surface accumulation of this reduced POM or a decomposition product may lead to electrode modification that causes electrode blockage. If indeed this does occur, then the resultant mass change should be detected by the EQCM technique via a change in the oscillation frequency of the quartz crystal working electrode [50].

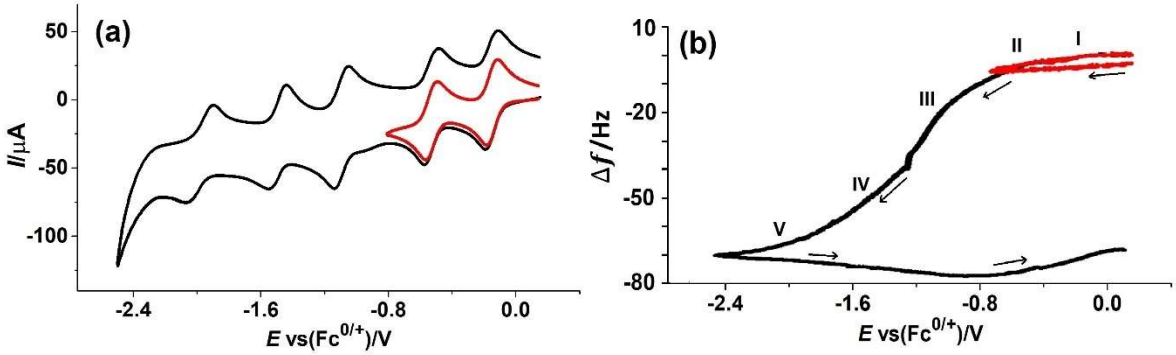

Figure 5. EQCM data obtained for the reduction of 1.0 mm α-$[S_2W_{18}O_{62}]^{4-}$ in CH_3CN (0.50 M [n-Bu_4N][PF_6]) at a scan rate of 0.050 V s^{-1} with an Au quartz crystal electrode over the potential region where the five (black) α-$[S_2W_{18}O_{62}]^{4-/5-/6-/7-/8-/9-}$ or the initial two α-$[S_2W_{18}O_{62}]^{4-/5-/6-}$ (red) processes occur. (a) DC cyclic voltammetry (current versus potential) and (b) change in frequency (Δf) of the gold quartz crystal versus potential.

In this study, the frequency (mass) change of a gold quartz crystal working electrode was monitored during the course of a DC cyclic voltammetric experiment (v = 0.050 V s^{-1}) undertaken with 1.0 mM α-$[S_2W_{18}O_{62}]^{4-}$ in CH_3CN (0.50 M [n-Bu_4N][PF_6]) over the potential region where five reduction processes occur (Figure 5a). Little change in mass accompanies processes I and II (Figure 5b). However, as also shown in Figure 5b, a significant

negative frequency shift, consistent with a mass increase, is evident at potentials corresponding to the onset of the 3rd α-$[S_2W_{18}O_{62}]^{6-/7-}$ reduction process and continues until the potential direction is reversed and the α-$[S_2W_{18}O_{62}]^{6-/5-/4-}$ oxidation processes occur where a small mass loss is detected. Apparently, accumulation of α-$[S_2W_{18}O_{62}]^{7-}$ itself, further reduced forms or their decomposition products occurs at a gold electrode. Probably, a related scenario applies at GC and Pt electrodes, but with electrode material dependent characteristics. This electrode surface accumulation phenomenon is not included in the modelling but would explain the diminution in the oxidation AC current components and asymmetry. Since surface accumulation continues to increase at potentials where α-$[S_2W_{18}O_{62}]^{7-}$ and even higher negatively charged species are generated, departures in experimental versus simulated data comparisons are anticipated to progressively increase for the α-$[S_2W_{18}O_{62}]^{7-/8-}$, α-$[S_2W_{18}O_{62}]^{8-/9-}$ and α-$[S_2W_{18}O_{62}]^{9-/10}$ processes which occur at more negative potentials and at longer times after the onset of the α-$[S_2W_{18}O_{62}]^{6-/7-}$ process. A mass increase and electrode blockage also was reported on the basis of EQCM data at a gold electrode in a recent study on the reduction of the $[n\text{-}Bu_4N]_4[PW_{11}O_{39}\{Sn(C_6H_4)C{\equiv}C(C_6H_4)(N_3C_4H_{10})\}]$ [12].

Results of 10 consecutive voltammetric experiments encompassing either reduction processes I and II or I, II and III at GC, Au and Pt electrodes in CH_3CN (0.50 M $[n\text{-}Bu_4N][PF_6]$) with 1.0 mM α-$[S_2W_{18}O_{62}]^{4-}$ are displayed in Figure 6, without polishing the electrode between experiments. If the potential range is limited to processes I and II, then each cyclic voltammetric experiment 1 to 10 remains essentially unchanged (Figures 6i-a, 6ii-a and 6iii-a). In contrast, when process III is included (see Figures 6i-b,c, 6ii-b,c and 6iii-b,c) each experiment displays a progressively enhanced level of change from peak (linear diffusion controlled) to sigmoidal shape (radial diffusion controlled) as also occurs in the voltammetry of metalloproteins or metalloenzymes [51-52] or with surface active diazonium modified POMs [12] when denaturation/decomposition and consequently surface blocking occur.

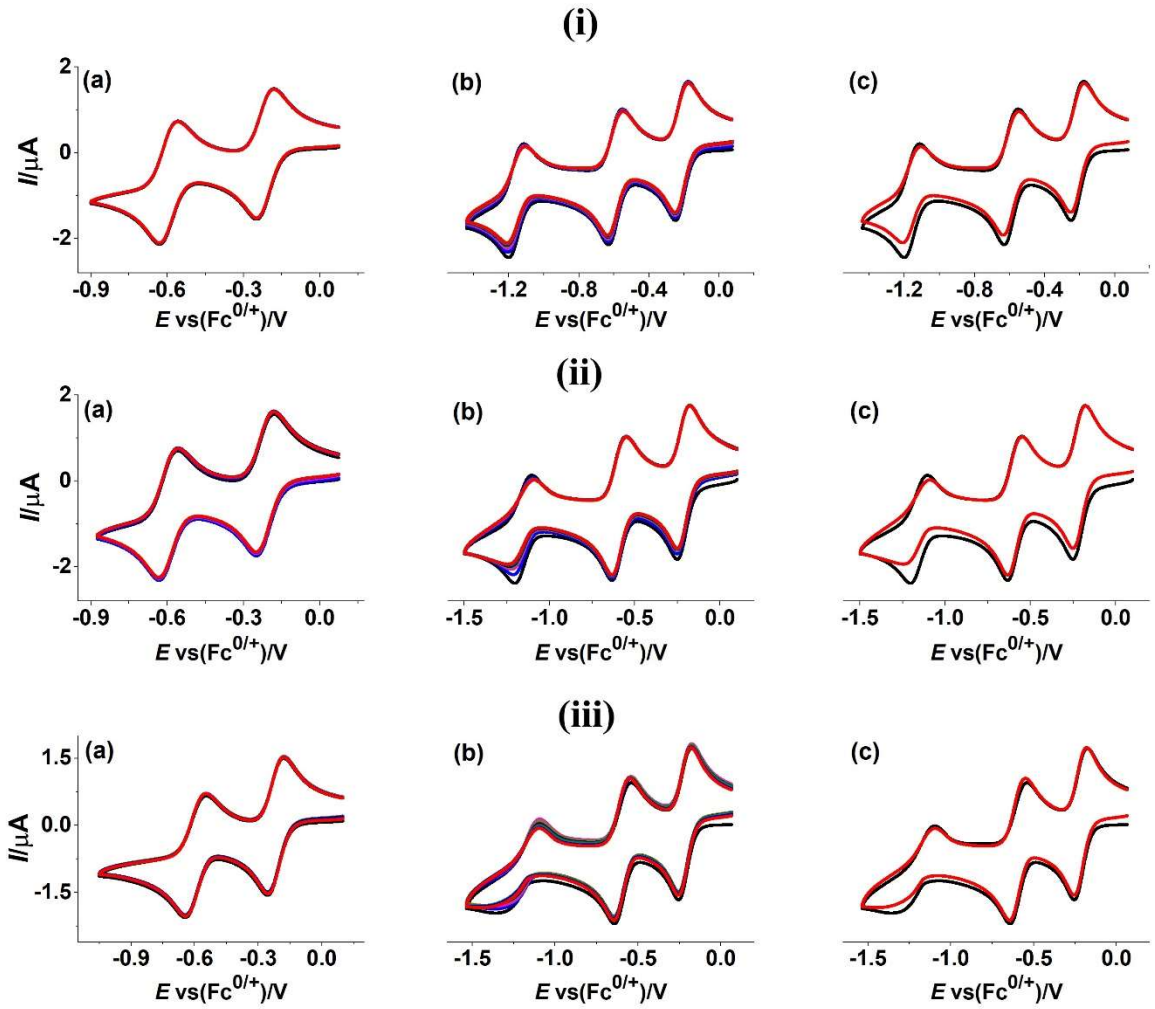

Figure 6. Repetitive cycling of the potential in voltammetry of 1.0 mM α-$[S_2W_{18}O_{62}]^{4-}$ in CH_3CN (0.50 M [n-Bu_4N][PF_6]) at (i) GC, (ii) Au and (iii) Pt electrodes without polishing the electrode after the first cycle. (a) and (b) encompass the potential region for processes I and II or I, II and III, respectively and (c) displays the 1st and 10th cycles of potential for processes I, II and III.

In a previous study, Richardt et al reported that only the initial two well-resolved processes were observed when 1.0 mM γ*-$[S_2W_{18}O_{62}]^{4-}$ is reduced in CH_3CN (0.10 M Bu_4NClO_4) [9] at a rotated GC electrode. The absence of processes at a more negative potential with use of this technique was postulated to be due to electrode blocking by formation of a surface confined product derived from the 2nd reduction process being more favourable at the

higher current densities associated with RDE voltammetry. The 3rd process was detectable with the addition of 5% water which was postulated to supress product accumulation. In contrast, RDE voltammetry in this work in CH_3CN (0.50 M [*n*-Bu_4N][PF_6]) with a higher electrolyte concentration and a lower 0.25 mM POM concentration allow six processes to be detected at a GC electrode (Figure 7a) with half wave potentials of -0.22, -0.61, -1.16, -1.54, -2.02, -2.37 V vs $Fc^{0/+}$ for processes I, II, III, IV, V and VI, respectively. However, electrode blocking is more pronounced at Au and Pt electrodes, resulting in only four (Figure 7b) or two well-defined processes (Figure 7c) respectively instead of the six obtained at the GC electrode.

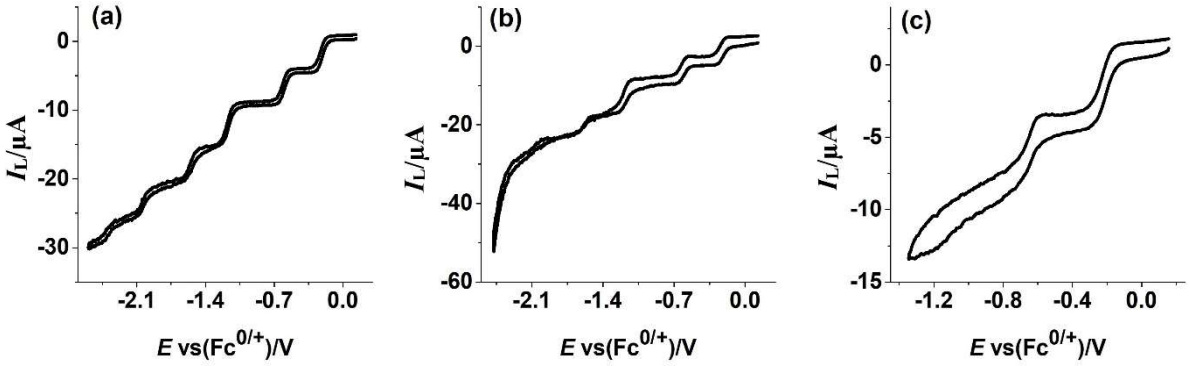

Figure 7. RDE voltammograms for the reduction of 0.25 mM α-$[S_2W_{18}O_{62}]^{4-}$ in CH_3CN (0.50 M [*n*-Bu_4N][PF_6]) at (a) GC, (b) BDD, (c) Au and (d) Pt electrodes. v = 0.050 V s^{-1}, rotation rate = 52.4 s^{-1}.

Based on evidence provided from DC voltammetry and EQCM experiments, it is apparent that significant surface accumulation and electrode blockage accompanies generation of the three-electron reduced α-$[S_2W_{18}O_{62}]^{7-}$ and further reduced forms with the order of impact being Pt > Au > GC. In contrast process I is not affected and process II only minimally modified by surface blockage. As a consequence of surface blockage, well-defined Pt electrode electrochemistry is restricted to first two process, with the third process being ill-defined. A voltammetric impact at the Au electrode of surface modification is the detection of asymmetry

in the reduction and oxidation current FTACV components, which is less extreme at the GC electrode and more extreme at the Pt electrode.

An understanding that the origin of at least some the asymmetry in FTACV is based on product accumulation justifies the emphasis in data analysis for estimation of k^0_{app} on the reduction component of the data set, as undertaken in the heuristic form of data analysis. Thus, this experimenter biased method generates what can be considered to be superior estimates of the electrode kinetic parameters. In principle, the automated data optimisation analysis approach also could be restricted to only the reduction data set to generate a new set of E^0_{app}, k^0_{app} and α_{app} values that would be anticipated to equate very closely with those generated via heuristic analysis. Using a heuristic data analysis method prior to implementation of automated data optimisation methods is again demonstrated to be highly valuable. The downside is that the heuristic approach is exceptionally tedious and time consuming for the experimenter. The challenge now is to implement artificial intelligence/ machine learning/ pattern recognition into data optimisation methods used in voltammetry that contain knowledge of the experimenter's experience in as has been implemented for simple problems [47-48].

In POM electrochemistry, the role ion-pairing must be significant. In this study, ion pairing between highly charged α-$[S_2W_{18}O_{62}]^{4-}$ or reduced species α-$[S_2W_{18}O_{62}]^{n-}$ (n = 5 to 10) and cation ($[n-Bu_4N]^+$) of the supporting electrolyte ([n-Bu_4N][PF_6]) will be enhanced the more negative the charge on the POM. Accordingly, the electron transfer process should be represented by a square-scheme mechanism which incorporates the coupling of ion-pairing with electron transfer [8, 46]. This mechanism also provides an explanation as to why k^0_{app} decreases with an increase in supporting electrolyte concentration as the $[n\text{-}Bu_4N]^+$ concentration is decreased from 0.50 M to 0.10 M. The combination of stronger ion pairing in the reduced relative to oxidised for a very sluggish POM processes as in a square reaction

scheme could in its own right explain the asymmetry in reduced and oxidised components of FTAC voltammetric data as noted in reference [8]. However, this study reveals that surface interaction features also contribute to and may even be the dominant contributor to this phenomenon. A positive shift in thermodynamically based E^0_{app} also is evident (see Table 1) with the higher 0.50 M concentration of supporting electrolyte ([n-Bu_4N][PF_6]), which is a consequence of enhanced ion-pairing differences between oxidised and reduced forms of each redox couple. Supporting electrolyte concentration dependency of ion pairing also has been established in previous studies of the electrochemistry of POMs [8, 43].

In this study, k^0_{app} for all processes at all electrode materials increased when the [n-Bu_4N][PF_6] supporting electrolyte concentration was decreased from 0.50 M to 0.10 M, which in part may be attributed to the diminution of the ion-pairing effect. The influence of the double layer region which contains a very high concentration of [n-Bu_4N]$^+$, particularly at the very negative potentials where processes IV, V and VI occur, also could be an important contributor to the increasingly sluggish electron transfer kinetics found as more electrons and hence negative charge are progressively added to the POM. The electrolyte concentration and potential dependent effect are related to the point of zero charge (PZC) which in turn is electrode material dependent [37]. It has been well established that even the oxidised forms of negatively charged POMs can adsorb spontaneously at carbon, Au and Pt electrodes [53-56]. The combination of very negative potentials where [n-Bu_4N]$^+$ concentrations in the double layer region are considerably higher than in bulk solution and extensive reduction leading to very high charges on the POMs may even provide scenarios where the solubility product is exceeded at the solution-electrode interface leading to precipitation of POM or specific adsorption of reduced POM which partially blocks the electrode and alters the mass transport thereby leading to departure from theoretical predictions based Butler-Volmer electrode kinetics and linear diffusion as found in this and other studies [12]. It needs to be remembered that the solubility

products of $[n\text{-Bu}_4\text{N}]^+$ salts of $[S_2W_{18}O_{62}]^{8-}$, $[S_2W_{18}O_{62}]^{9-}$ or $[S_2W_{18}O_{62}]^{10-}$ for example have a $[n\text{-Bu}_4\text{N}]^+$ concentration term raised to the power 8, 9 and 10 respectively. In the presence of very high $[n\text{-Bu}_4\text{N}]^+$ concentrations at the electrode interface, precipitation (electrocrystallisation) of a POM salt onto the electrode surface is likely to be thermodynamically very favourable.

Unfortunately, the PZC value at GC, Au and Pt electrodes has not been established, although at potentials more negative than process II should almost certainly be more negative than the PZC and hence provide conditions favouring a $[n\text{-Bu}_4\text{N}]^+$ dominated double layer region. However, studies by Fawcett et al [18] are available on the double layer at the mercury electrode-acetonitrile interface where the PZC is known. This work provides details of the potential dependence of the electrolyte cation (tetraalkylammonium) distribution in the mercury electrode-solution double layer interfacial region. As expected, the double layer effect leads to enhanced tetraalkylammonium concentration the more negative the potential is relative to the PZC. Thus, the α-$[S_2W_{18}O_{62}]^{9-/10-}$ process at very negative potentials should be influenced more by the double layer effect compared to α-$[S_2W_{18}O_{62}]^{4-/5-}$ process which may be near to the PZC and there should be an electrode dependent progressive increase in complexity for processes the more negative their reversible potential.

4. CONCLUSION

E^0 (reversible formal potential), k^0 (heterogeneous charge transfer rate constant) at E^0 and α (charge transfer coefficient) for up to six α-$[S_2W_{18}O_{62}]^{4-}$ reduction processes have been determined in acetonitrile containing 0.50 or 0.10 M $[n\text{-Bu}_4\text{N}][PF]$ as the supporting electrolyte at GC, Au and Pt macrodisc electrodes by FTAC voltammetry using both heuristic and computer-assisted automated data analysis approaches. Under all conditions, the k^0 values

determined by use of the Butler-Volmer model of electron transfer lie in the order GC (close to reversible) >Au > Pt (sluggish kinetics) despite the fact that the density of states at Pt is significantly higher [44], suggesting an inner-sphere nature of these processes. k^0 values also increased on lowering the [*n*-Bu4N][PF_6] supporting electrolyte concentration from 0.50 to 0.10 M, due to the decrease in solvent viscosity at lower electrolyte concentration. This electrolyte dependent k^0 probably is also the result of a decrease in ion-pairing that is not included in the modelling [46]. The level of agreement between simulated data derived from the Butler-Volmer relationship progressively decreased the more extensive the level of reduction in the α-$[S_2W_{18}O_{62}]^{4-/5-/6-/7-/8-/9-/10-}$ series of processes. This non-ideality led to differences in electrode kinetic values being reported when using heuristic experimenter controlled parameterisation and computer based automated data optimisation. EQCM experiments at a gold quartz crystal electrode and repetitive DC cyclic voltammetric experiments at GC, Au and Pt electrodes demonstrate that surface accumulation of reduced species detected as a mass increase also is a significant contributor to departures from the Butler-Volmer model with mass transport by linear diffusion. Surface accumulation becomes significant at the onset of the third reduction process and increases as the potential becomes more negative, which mimics the progressive departures in experimental versus simulated data comparisons that occur in the α-$[S_2W_{18}O_{62}]^{4-/5-/6-/7-/8-/9-/10-}$ reduction sequence. Another factor contributing to progressive complexity is the double layer effect, which is electrode material dependent and becomes larger the more negative potential is relative to the PZC. This effect can lead to very high [*n*-Bu4N]$^+$ concentrations at the electrode-solution interface and is also expected to be more influential for α-$[S_2W_{18}O_{62}]^{9-/10}$ process that occurs at very negative potentials than for α-$[S_2W_{18}O_{62}]^{4-/5-}$ process which is probably relatively close to the PZC. It is even plausible that the solubility product for the [*n*-Bu4N]$^+$

salts of extensively reduced POMs is exceeded. The findings in this study are expected to apply to the reduction of other very negatively charged POMs.

ASSOCIATED CONTENT

Supporting Information

Formal reversible potentials (E_f^0)[a] and other data reported for the reduction of α-$[S_2W_{18}O_{62}]^{4-}$ (**Table S1**); Comparison of simulated and experimental FTAC voltammetric data derived from reduction of 2.5 mM α $[S_2W_{18}O_{62}]^{4-}$ in CH_3CN containing 0.50 M [*n*-Bu_4N][PF_6] at GC, Au and Pt electrodes (**Figures S1-4**); Comparison of simulated and experimental FTAC voltammetric data derived from reduction of 2.5 mM α $[S_2W_{18}O_{62}]^{4-}$ in CH_3CN containing 0.10 M [*n*-Bu_4N][PF_6] at GC, Au and Pt electrodes (**Figures S4-8**).

AUTHOR INFORMATION

Corresponding Authors

Alan M. Bond - School of Chemistry and ARC Centre of Excellence for Electrochemical Science, Monash University, Clayton, Victoria 3800, Australia; ORCID: orcid.org/0000-0002-1113-5205; Email: alan.bond@monash.edu

Jie Zhang - School of Chemistry and ARC Centre of Excellence for Electrochemical Science, Monash University, Clayton, Victoria 3800, Australia; ORCID: orcid.org/0000-0003-2493-5209; Email: jie.zhang@monash.edu

Authors

Md Anisur Rahman - School of Chemistry, Monash University, Clayton, Victoria 3800, Australia; Email: anisur.rahman@monash.edu

Luke Gundry - School of Chemistry, Monash University, Clayton, Victoria 3800, Australia; Email: luke.gundry1@monash.edu

Tadaharu Ueda - Department of Marine Resource Science, Faculty of Agriculture and Marine Science, Kochi University, Kochi 780-8520, Email: chuji@kochi-u.ac.jp

ACKNOWLEDGMENT

The authors thank the Australian Research Council for financial assistance provided by the award of a Discovery Program grant.

REFERENCES

1. Li, J.; Guo, S.-X.; Bentley, C. L.; Bano, K.; Bond, A. M.; Zhang, J.; Ueda, T. Electrode Material Dependence of the Electron Transfer Kinetics Associated with the [$[SVW_{11}O_{40}]^{3-/4-}$($V^{V/IV}$) and $[SVW_{11}O_{40}]^{4-/5-}$ ($W^{VI/V}$) Processes in Dimethylformamide. *Electrochim. Acta* **2016**, *201*, 45-56.
2. Nambu, J.-i.; Ueda, T.; Guo, S.-X.; Boas, J. F.; Bond, A. M. Detailed Voltammetric and Epr Study of Protonation Reactions Accompanying the One-Electron Reduction of Keggin-Type Polyoxometalates, $[XV^{V}M_{11}O_{40}]^{4-}$(X= P, As; M= Mo, W) in Acetonitrile. *Dalton Trans.* **2010**, *39*, 7364-7373.
3. López, X.; Carbó, J. J.; Bo, C.; Poblet, J. M. Structure, Properties and Reactivity of Polyoxometalates: A Theoretical Perspective. *Chem. Soc. Rev.* **2012**, *41*, 7537-7571.
4. Poblet, J. M.; López, X.; Bo, C. Ab Initio and Dft Modelling of Complex Materials: Towards the Understanding of Electronic and Magnetic Properties of Polyoxometalates. *Chem. Soc. Rev.* **2003**, *32*, 297-308.
5. Ueda, T. Electrochemistry of Polyoxometalates: From Fundamental Aspects to Applications. *ChemElectroChem* **2018**, *5*, 823-838.
6. Way, D. M.; Bond, A. M.; Wedd, A. G. Multielectron Reduction of α-$[S_2Mo_{18}O_{62}]^{4-}$ in Aprotic and Protic Media: Voltammetric Studies. *Inorg. Chem.* **1997**, *36*, 2826-2833.
7. Zhang, J.; Bond, A. M.; MacFarlane, D. R.; Forsyth, S. A.; Pringle, J. M.; Mariotti, A. W.; Glowinski, A. F.; Wedd, A. G. Voltammetric Studies on the Reduction of Polyoxometalate Anions in Ionic Liquids. *Inorg. Chem.* **2005**, *44*, 5123-5132.
8. Rahman, M. A.; Li, J.; Guo, S.-X.; Kennedy, G.; Ueda, T.; Bond, A. M.; Zhang, J. Modelling Limitations Encountered in the Thermodynamic and Electrode Kinetic Parameterization of the α-$[S_2W_{18}O_{62}]^{4-/5-/6-}$ Processes at Glassy Carbon and Metal Electrodes. *J. Electroanal. Chem.* **2019**, 113786.
9. Richardt, P. J.; Gable, R. W.; Bond, A. M.; Wedd, A. G. Synthesis and Redox Characterization of the Polyoxo Anion, γ*-$[S_2W_{18}O_{62}]^{4-}$: A Unique Fast Oxidation Pathway Determines the Characteristic Reversible Electrochemical Behavior of Polyoxometalate Anions in Acidic Media. *Inorg. Chem.* **2001**, *40*, 703-709.
10. Zhang, J.; Bond, A. M.; Richardt, P. J.; Wedd, A. G. Voltammetric Reduction of α- and γ-$[S_2W_{18}O_{62}]^{4-}$ and α-, β- and γ-$[S_2W_{18}O_{62}]^{4-}$: Isomeric Dependence of Reversible Potentials of Polyoxometalate Anions Using Data Obtained by Novel Dissolution and Conventional Solution-Phase Processes. *Inorg. Chem.* **2004**, *43*, 8263-8271.
11. Rahman, M. A. Mechanistic Subtleties in the Voltammetry of Polyoxometalates. Ph.D. Dissertation, Monash University, **2020**.
12. Rahman, M. A.; Guo, S.-X.; Laurans, M.; Izzet, G.; Proust, A.; Bond, A. M.; Zhang, J. Thermodynamics, Electrode Kinetics and Mechanistic Nuances Associated with the Voltammetric Reduction of Dissolved $[n\text{-}Bu_4N]_4[PW_{11}O_{39}\{Sn(C_6H_4)C\equiv C(C_6H_4)(N_3C_4H_{10})\}]$ and a Surface Confined Diazonium Derivative. *ACS Appl. Energy Mater.* **2020**, 3991-4006.
13. Fullmer, L. B.; Molina, P. I.; Antonio, M. R.; Nyman, M. Contrasting Ion-Association Behaviour of Ta and Nb Polyoxometalates. *Dalton Trans.* **2014**, *43*, 15295-15299.
14. Gómez-Gil, J.; Laborda, E.; Gonzalez, J.; Molina, A.; Compton, R. Electrochemical and Computational Study of Ion Association in the Electroreduction of $PW_{12}O_{40}^{3-}$. *J. Phys. Chem. C* **2017**, *121*, 26751-26763.

15. Sures, D. J.; Serapian, S. A.; Kozma, K.; Molina, P. I.; Bo, C.; Nyman, M. Electronic and Relativistic Contributions to Ion-Pairing in Polyoxometalate Model Systems. *Phys. Chem. Chem. Phys.* **2017**, *19*, 8715-8725.

16. Lucio, A. J.; Shaw, S. K.; Zhang, J.; Bond, A. M. Large-Amplitude Fourier-Transformed Ac Voltammetric Study of the Capacitive Electrochemical Behavior of the 1-Butyl-3-Methylimidazolium Tetrafluoroborate–Polycrystalline Gold Electrode Interface. *J. Phys. Chem. C* **2017**, *121*, 12136-12147.

17. Silva, F.; Gomes, C.; Figueiredo, M.; Costa, R.; Martins, A.; Pereira, C. M. The Electrical Double Layer at the [Bmim][PF_6] Ionic Liquid/Electrode Interface–Effect of Temperature on the Differential Capacitance. *J. Electroanal. Chem.* **2008**, *622*, 153-160.

18. Fawcett, W.; Loutfy, R. Double Layer Structure at the Mercury/Acetonitrile Interface. *Can. J. Chem.* **1973**, *51*, 230-236.

19. Müller, A.; Dloczik, L.; Diemann, E.; Pope, M. T. A Cyclic Voltammetric Study of Mangano (Ii) Undecatungstosilicate: An Illustrative Example of the Reduction, Protonation and Disproportionation Pathways of Transition Metal Substituted Heteropolytungstates in Aqueous Solution. *Inorg. Chim. Acta* **1997**, *257*, 231-239.

20. Bond, A. M. *Broadening Electrochemical Horizons*; Oxford Press: New York, 2002.

21. Geletii, Y. V.; Botar, B.; Kögerler, P.; Hillesheim, D. A.; Musaev, D. G.; Hill, C. L. An All‐Inorganic, Stable, and Highly Active Tetraruthenium Homogeneous Catalyst for Water Oxidation. *Angew. Chem. Int. Ed.* **2008**, *47*, 3896-3899.

22. Guo, S.-X.; Liu, Y.; Lee, C.-Y.; Bond, A. M.; Zhang, J.; Geletii, Y. V.; Hill, C. L. Graphene-Supported [{$Ru_4O_4(OH)_2(H_2O)_4$}(γ-$SiW_{10}O_{36})_2$]$^{10-}$ for Highly Efficient Electrocatalytic Water Oxidation. *Energy Environ. Sci.* **2013**, *6*, 2654-2663.

23. Kozhevnikov, I. V. Catalysis by Heteropoly Acids and Multicomponent Polyoxometalates in Liquid-Phase Reactions. *Chem. Rev.* **1998**, *98*, 171-198.

24. Mizuno, N.; Yamaguchi, K.; Kamata, K. Epoxidation of Olefins with Hydrogen Peroxide Catalyzed by Polyoxometalates. *Coord. Chem. Rev.* **2005**, *249*, 1944-1956.

25. Wang, D.; Liu, L.; Jiang, J.; Chen, L.; Zhao, J. Polyoxometalate-Based Composite Materials in Electrochemistry: State-of-the-Art Progress and Future Outlook. *Nanoscale* **2020**, *12*, 5705-5718.

26. Hou, Y.; Chai, D.; Li, B.; Pang, H.; Ma, H.; Wang, X.; Tan, L. Polyoxometalate-Incorporated Metallacalixarene@Graphene Composite Electrodes for High-Performance Supercapacitors. *ACS Appl. Mater. Interfaces* **2019**, *11*, 20845-20853.

27. Chen, J. J.; Symes, M. D.; Fan, S. C.; Zheng, M. S.; Miras, H. N.; Dong, Q. F.; Cronin, L. High‐Performance Polyoxometalate‐Based Cathode Materials for Rechargeable Lithium‐Ion Batteries. *Adv. Mater.* **2015**, *27*, 4649-4654.

28. Pratt III, H. D.; Anderson, T. M. Mixed Addenda Polyoxometalate “Solutions” for Stationary Energy Storage. *Dalton Trans.* **2013**, *42*, 15650-15655.

29. Pratt III, H. D.; Hudak, N. S.; Fang, X.; Anderson, T. M. A Polyoxometalate Flow Battery. *J. Power Sources* **2013**, *236*, 259-264.

30. Pratt III, H. D.; Pratt, W. R.; Fang, X.; Hudak, N. S.; Anderson, T. M. Mixed-Metal, Structural, and Substitution Effects of Polyoxometalates on Electrochemical Behavior in a Redox Flow Battery. *Electrochim. Acta* **2014**, *138*, 210-214.

31. Himeno, S.; Tatewaki, H.; Hashimoto, M. Synthesis, Structure, and Characterization of an α-Dawson-Type [$S_2W_{18}O_{62}$]$^{4-}$ Complex. *Bull. Chem. Soc. Jpn.* **2001**, *74*, 1623-1628.

32. Sawyer, D.; Sobkowiak, A.; Roberts Jr, J. *Electrochemistry for Chemists*; 2nd eds.; Wiley: New York, 1995; pp 358-402.

33. Bond, A. M.; Duffy, N. W.; Guo, S.-X.; Zhang, J.; Elton, D. Changing the Look of Voltammetry. *Anal. Chem.* **2005**, 186A-195A.
34. Sher, A. A.; Bond, A. M.; Gavaghan, D. J.; Harriman, K.; Feldberg, S. W.; Duffy, N. W.; Guo, S.-X.; Zhang, J. Resistance, Capacitance, and Electrode Kinetic Effects in Fourier-Transformed Large-Amplitude Sinusoidal Voltammetry: Emergence of Powerful and Intuitively Obvious Tools for Recognition of Patterns of Behavior. *Anal. Chem.* **2004**, *76*, 6214-6228.
35. Zhang, J.; Guo, S.-X.; Bond, A. M.; Marken, F. Large-Amplitude Fourier Transformed High-Harmonic Alternating Current Cyclic Voltammetry: Kinetic Discrimination of Interfering Faradaic Processes at Glassy Carbon and at Boron-Doped Diamond Electrodes. *Anal. Chem.* **2004**, *76*, 3619-3629.
36. Gritzner, G.; Kuta, J. Recommendations on Reporting Electrode Potentials in Nonaqueous Solvents (Recommendations 1983). *Pure. Appl. Chem.* **1984**, *56*, 461-466.
37. Bard, A. J.; Faulkner, L. R. *Electrochemical Methods: Fundamentals and Applications*, 2nd eds.; Wiley: New York, 2001.
38. Zhang, J.; Guo, S.-X.; Bond, A. M. Discrimination and Evaluation of the Effects of Uncompensated Resistance and Slow Electrode Kinetics from the Higher Harmonic Components of a Fourier Transformed Large-Amplitude Alternating Current Voltammogram. *Anal. Chem.* **2007**, *79*, 2276-2288.
39. Kennedy, G. F., MECSim Software Package. http://www.garethkennedy.net/MECSim.html, 2019 (accessed June 2020).
40. Bond, A. M.; Duffy, N. W.; Elton, D. M.; Fleming, B. D. Characterization of Nonlinear Background Components in Voltammetry by Use of Large Amplitude Periodic Perturbations and Fourier Transform Analysis. *Anal. Chem.* **2009**, *81*, 8801-8808.
41. Liu, Y. P.; Guo, S.-X.; Bond, A. M.; Zhang, J.; Geletii, Y. V.; Hill, C. L. Voltammetric Determination of the Reversible Potentials for $[\{Ru_4O_4(OH)_2(H_2O)_4\}(\gamma\text{-}SiW_{10}O_{36})_2]^{10-}$ over the Ph Range of 2-12: Electrolyte Dependence and Implications for Water Oxidation Catalysis. *Inorg. Chem.* **2013**, *52*, 11986-11996.
42. Guo, S.-X.; Feldberg, S. W.; Bond, A. M.; Callahan, D. L.; Richardt, P. J. S.; Wedd, A. G. Systematic Approach to the Quantitative Voltammetric Analysis of the Fe^{III}/Fe^{II} Component of the α_2-$[Fe(OH)_2P_2W_{17}O_{61}]^{7-/8-}$ Reduction Process in Buffered and Unbuffered Aqueous Media. *J. Phys. Chem. B* **2005**, *109*, 20641-20651.
43. Li, J.; Bentley, C. L.; Bond, A. M.; Zhang, J.; Ueda, T. Influence of 1-Butyl-3-Methylimidazolium on the Electron Transfer Kinetics Associated with the $[SVW_{11}O_{40}]^{3-/4-}$($V^{V/IV}$) and $[SVW_{11}O_{40}]^{4-/5-}$($W^{VI/V}$) Processes in Dimethylformamide. *J. Electroanal. Chem.* **2016**, *779*, 67-74.
44. Bano, K.; Zhang, J.; Bond, A. M.; Unwin, P. R.; Macpherson, J. V. Diminished Electron Transfer Kinetics for $[Ru(NH_3)_6]^{3+/2+}$, $[\alpha\text{-}SiW_{12}O_{40}]^{4-/5-}$, and $[\alpha\text{-}SiW_{12}O_{40}]^{5-/6-}$ Processes at Boron-Doped Diamond Electrodes. *J. Phys. Chem. C* **2015**, *119*, 12464-12472.
45. Guo, S.-X.; Bond, A. M.; Zhang, J. Fourier Transformed Large Amplitude Alternating Current Voltammetry: Principles and Applications. *Rev. Polarogr.* **2015**, *61*, 21-32.
46. Li, J.; Bond, A. M.; Zhang, J. Probing Electrolyte Cation Effects on the Electron Transfer Kinetics of the $[\alpha\text{-}SiW_{12}O_{40}]^{4-/5-}$, and $[\alpha\text{-}SiW_{12}O_{40}]^{5-/6-}$ Processes Using a Boron-Doped Diamond Electrode. *Electrochim. Acta* **2015**, *178*, 631-637.
47. Stephenson, M.; Amarasinghe, S.; Martin, M.; O'Reilly, U.-M. Meta Optimization: Improving Compiler Heuristics with Machine Learning. *ACM sigplan notices* **2003**, *38*, 77-90.

48. Kennedy, G. F.; Zhang, J.; Bond, A. M. Automatically Identifying Electrode Reaction Mechanisms Using Deep Neural Networks. *Anal. Chem.* **2019**, *91*, 12220-12227.
49. Bentley, C. L.; Li, J. Z.; Bond, A. M.; Zhang, J. Mass-Transport and Heterogeneous Electron-Transfer Kinetics Associated with the Ferrocene/Ferrocenium Process in Ionic Liquids. *J. Phys. Chem. C* **2016**, *120*, 16516-16525.
50. Sauerbrey, G. The Use of Quarts Oscillators for Weighing Thin Layers and for Microweighing. *Z. Phys.* **1959**, *155*, 206-222.
51. Bogdanovskaya, V.; Tarasevich, M.; Hintsche, R.; Scheller, F. Electrochemical Transformations of Proteins Adsorbed at Carbon Electrodes. *Bioelectrochem. Bioenerg.* **1988**, *19*, 581-584.
52. Salvatore, P.; Zeng, D.; Karlsen, K. K.; Chi, Q.; Wengel, J.; Ulstrup, J. Electrochemistry of Single Metalloprotein and DNA‐Based Molecules at Au (111) Electrode Surfaces. *ChemPhysChem* **2013**, *14*, 2101-2111.
53. Choi, S.-H.; Kim, J.-W. Adsorption Properties of Keggin-Type Polyoxometalates on Carbon Based Electrode Surfaces and Their Electrocatalytic Activities. *Bull. Korean Chem. Soc.* **2009**, *30*, 810-816.
54. Guo, Z. P.; Han, D. M.; Wexler, D.; Zeng, R.; Liu, H. K. Polyoxometallate-Stabilized Platinum Catalysts on Multi-Walled Carbon Nanotubes for Fuel Cell Applications. *Electrochim. Acta* **2008**, *53*, 6410-6416.
55. Rong, C.; Anson, F. C. Spontaneous Adsorption of Heteropolytungstates and Heteropolymolybdates on the Surfaces of Solid Electrodes and the Electrocatalytic Activity of the Adsorbed Anions. *Inorg. Chim. Acta* **1996**, *242*, 11-16.
56. Wang, B.; Dong, S. Electrochemical Study of Isopoly-and Heteropoly-Oxometallates Film Modified Microelectrodes—Vi. Preparation and Redox Properties of 12-Molybdophosphoric Acid and 12-Molybdosilicic Acid Modified Carbon Fiber Microelectrodes. *Electrochim. Acta* **1996**, *41*, 895-902.

TOC:

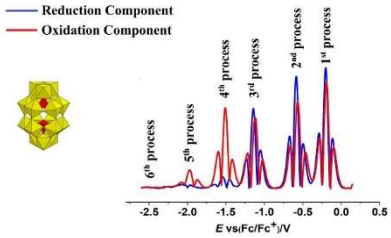
Reduction Component
Oxidation Component
6th process
5th process
4th process
3rd process
2nd process
1st process
-2.5
-2.0
-1.5
-1.0
-0.5
0.0
0.5
E vs(Fc/Fc+)/V